Article

Impacts of Leaf Age on Canopy Spectral Signature Variation in Evergreen Chinese Fir Forests

Qiaoli Wu [1,2]**, Conghe Song** [3] **, Jinling Song** [1,2,*]**, Jindi Wang** [1,2] **, Shaoyuan Chen** [1,2] **and Bo Yu** [1,2]

[1] State Key Laboratory of Remote Sensing Science, Jointly Sponsored by Beijing Normal University and Institute of Remote Sensing and Digital Earth of Chinese Academy of Sciences, Beijing 100875, China; wuql@mail.bnu.edu.cn (Q.W.); wangjd@bnu.edu.cn (J.W.); chenshaoyuan1020@gmail.com (S.C.); yuboray@163.com (B.Y.)

[2] Beijing Engineering Research Center for Global Land Remote sensing Products, Institute of Remote Sensing Science and Engineering, Faculty of Geographical Science, Beijing Normal University, Beijing 100875, China

[3] Department of Geography, University of North Carolina at Chapel Hill, Chapel Hill, NC 27599, USA; csong@email.unc.edu

* Correspondence: songjl@bnu.edu.cn; Tel.: +86-10-5880-5452; Fax: +86-10-5880-5274

Abstract: Significant gaps exist in our knowledge of the impact of leaf aging on canopy signal variability, which limits our understanding of vegetation status based on remotely sensed data. To understand the effects of leaf aging at the leaf and canopy scales, a combination of field, remote-sensing and physical modeling techniques was adopted to assess the canopy spectral signals of evergreen *Cunninghamia* forests. We observed an approximately 10% increase in Near-Infrared (NIR) reflectance for new leaves and a 35% increase in NIR transmittance for mature leaves from May to October. When variations in leaf optical properties (LOPs) of only mature leaves, or both new and mature leaves were considered, the Geometric Optical and Radiative Transfer (GORT) model-simulated canopy reflectance trajectory was more consistent with Landsat observations (R^2 increased from 0.37 to 0.82~0.89 for NIR reflectance, and from 0.35 to 0.67~0.88 for EVI2, with a small RMSE (0.01 to 0.02)). This study highlights the importance of leaf age on leaf spectral signatures, and provides evidence of age-dependent LOPs that have important impacts on canopy reflectance in the NIR band and EVI2, which are used to monitor canopy dynamics and productivity, with important implications for RS and forest ecosystem ecology.

Keywords: leaf age; leaf spectral properties; leaf area index; *Cunninghamia*; Chinese fir; canopy reflectance; NIR; EVI2; geometric optical radiative transfer (GORT) model

1. Introduction

Forests cover approximately 30% of the Earth's land area (4.2×10^9 hectares). Globally, forests play critical roles in providing goods and services for terrestrial ecosystems, including filtering water, controlling water runoff, protecting soil, regulating the climate, and cycling and storing nutrients [1,2]. Many important biophysical processes in forests are conducted through leaves, including photosynthesis, transpiration, respiration, and light interception. Forests and other land vegetation currently remove approximately 30% of anthropogenic CO_2 emissions from the atmosphere through photosynthesis [3–5]. While high value has been placed on remote sensing (RS) for ecological research, management and modeling of forest canopy status at an ecosystem scale, a concomitant increase in understanding the factors that affect canopy reflectance has been only partially realized.

The interpretation of RS signals for forest canopies requires profound knowledge of the factors affecting their optical properties, which may be internal or external to the forest stand [6]. To extract

useful information related to canopy growth using time-series data, anomalies in time-series data that are unrelated to real changes in canopies should be eliminated, such as clouds and aerosol contamination [7,8] as well as bidirectional reflectance distribution function (BRDF) effects caused by topography and sun-sensor geometry variation [9–14]. Abundant studies have confirmed the existence of significant seasonal patterns in the optical RS signal trajectory that remain after removing the impacts of these factors external to the forest stand [11,13,15,16]. Thus, variations in reflectance trajectories contain useful information related to factors internal to the stand. Based on previously reported experimental and modeling data, vegetation reflectance is primarily a function of tissue optical properties (reflectance and transmittance), canopy biophysical attributes (e.g., leaf area, foliage clumping) and background reflectance [17–21]. Leaf optical properties (LOPs) and leaf area index (LAI) are two of the main recognized internal factors involved in controlling canopy reflectance.

Seasonality in canopy spectral signals has been attributed to a varying LAI along with new leaf development and defoliation [22]. In deciduous forests, LAI shows high seasonality and might be the most significant factor affecting canopy reflectance, as all leaves are shed in winter. However, the situation is very different for mature evergreen forests, which show a relatively stable total leaf area every year. Thus, changes in canopy reflectance do not necessarily imply changes in LAI [23]. In evergreen forests, leaves have more than a one-year lifespan, and current-year new leaves remain throughout the winter. Although old leaves are shed every year, new leaves are also produced every year. The total leaf area in evergreen forests remains relatively stable throughout a year compared with deciduous forests. However, we still find significant seasonal variation in canopy reflectance in evergreen forests, which may not be caused by variations in LAI but rather by other internal factors. Further studies are needed to develop a more profound interpretation of the seasonality of optical RS signals for evergreen forests.

In addition to leaf area, LOPs are another significant factor that can change with time, which may strongly affect canopy reflectance [19,23,24], and leaf-age effects on canopy signals require more attention. Leaves affects the radiation field through its LOPs, including leaf reflectance and transmittance characteristics, which are wavelength-dependent [25,26]. A few supporting studies have confirmed the combined effects of LAI and LOPs on the seasonality of gross ecosystem CO_2 exchange (GEE), photosynthesis and NIR reflectance for Amazonian forests [23,27,28]. Many efforts aimed at accounting for effect of stand age on canopy reflectance with forest succession have improved the interpretation of canopy signals [29–33]. However, only a few studies have indicated that in addition to stand age, leaf age might also have a significant impact. Our ability to both interpret RS signals and develop new RS technologies for vegetation depends directly on our ability to resolve the multitude of factors controlling canopy and landscape reflectance signatures. This situation inspired us to further evaluate robust biophysical interpretations of the seasonality of optical RS signals, with a focus on evergreen forests, by examining the effects of age-dependent leaf properties on canopy reflectance.

Different age cohorts of leaves coexist in the canopy of evergreen forests, which can be classified to two main age groups: current-year new leaves (≤1 a) and mature leaves (>1 a), which might exhibit different LOPs and, thus, different impacts on canopy reflectance. Mature leaves represent the majority and new leaves are the minority of leaves flushed every year. On the other hand, new leaves are mainly distributed at the top and in the outermost parts in tree crowns, while mature leaves are distributed in the lower and inner parts of the canopy. Thus, the seasonal variation of canopy reflectance might be strongly affected by changes in LOPs of both new leaves and mature leaves. This brings us to the crux of our study: the quantitative analysis and interpretation of the different leaf-aging effects of new leaves and mature leaves on seasonal variations in canopy reflectance. Hence, we addressed the following research questions in this study: (1) how do the LOPs of new leaves and mature leaves vary during the leaf maturation process? (2) How should the contributions of new leaves and mature leaves to canopy optical properties be quantified? (3) How does leaf aging affect the seasonal variation of the remotely sensed response spectral signals of evergreen forest canopies?

2. Materials

2.1. Study Sites

This study focused on two National Research Stations of Forest Ecosystems in Huitong county, Hunan province, China, as shown in Figure 1. The first station (Station 1, S1) is located at 26°40′N, 109°26′E, and the second station (Station 2, S2) is located at 26°50′N, 109°45′E. S1 was established in 1983, and S2 was established in 1996. Two main permanent sampling plots, ZH1 and WS3, were selected from S1 and S2, respectively, to measure and evaluate the effects of leaf aging on canopy optical properties. Two additional auxiliary plots, i.e., FZ1 and WS2, were also selected for comparison with the main plots. FZ1 exhibits the same plot conditions as ZH1 but is smaller, with a size of 30 × 40 m. WS3 is located next to WS2 and is eight years older than WS2.

Cunninghamia (Chinese fir) is a fast growing species, with its height increasing as much as 1 m per year [34], and usually matures approximately 20 a. The same *Cunninghamia* seedlings were planted in ZH1 and FZ1 after clear cutting. The stem density is the same in ZH1/FZ1, which exhibits half the density in WS2 (1920 trees ha^{-1}) and WS3 (1967 trees ha^{-1}). ZH1/FZ1 were planted with an initial stem density of 2500 trees ha^{-1} and thinned twice, once in 1997 and again in 2003, to a stable density of 1035 trees ha^{-1}.
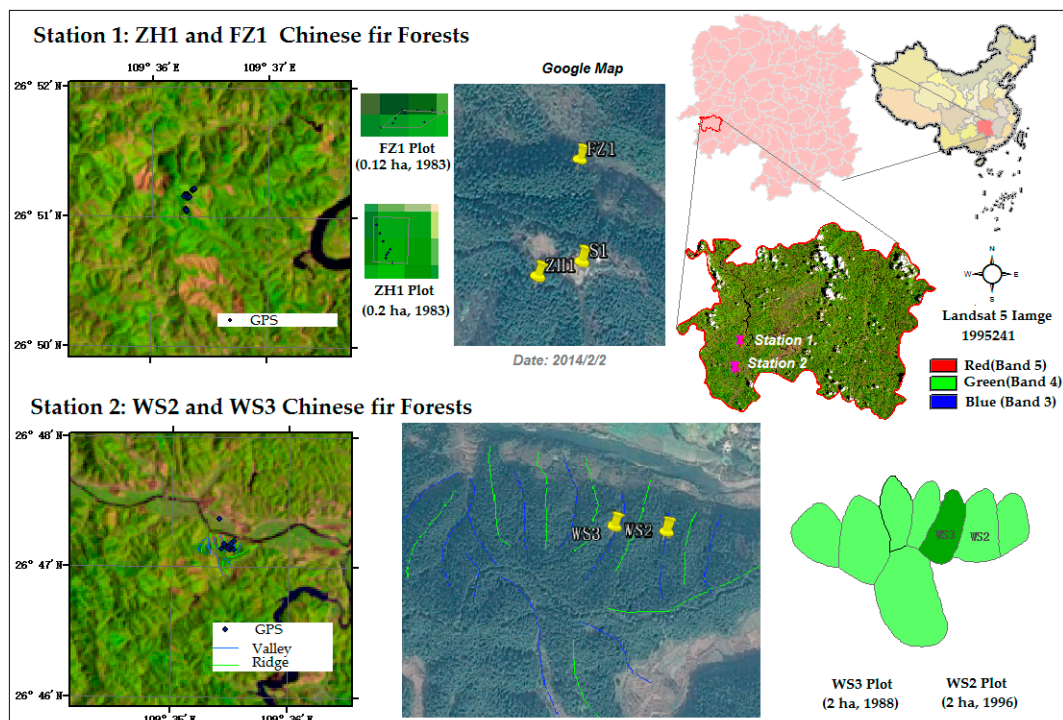

Figure 1. These four study plots are covered by *Cunninghamia lanceolata* (also known as Chinese fir) plantations, which were replanted after clear-cutting.

2.2. Field Data

2.2.1. Canopy Structural Parameter Measurements

Crown shape measurements were taken from a total of forty trees in S2. The size of the selected trees was evenly distributed in terms of height (*H*) (from 5.4 m to 20 m) and diameter at breast height (DBH) (from 7.7 cm to 37.8 cm). Among the 40 trees, seven trees were located in plots close to the study site, and 33 trees were located within sites ZH1 and FZ1. The parameters measured for the characterization of crown shape included the following: crown width in the north-south direction (*R*1) and the east-west direction (*R*2), tree height (*H*1) and height under the crown (*H*2), from which we can obtain the height

of the crown center (*h*). A detailed description of the crown shape measurements can be found in Appendix A.

Only DBH and *H*1 were measured annually for each tree in the study plots, and other canopy structure parameters were only measured once for the 40 trees. Hence, to characterize the dominant stand canopy structure changes with time, we needed to build allometric relationships between other unknown canopy structural parameters with DBH or *H*1. The derived canopy structure parameters included the following:

- Crown radius (*R*): $R = (1.296 + 0.146 * \text{DBH})/2$, $R^2 = 0.76$, RMSE = 0.72;
- Full tree height (*H*1): $H1 = 3.928 + 14.866 * (1 - \exp(-0.1865 * \text{DBH}^{8.285}))$, $R^2 = 0.94$, RMSE = 1.30;
- Crown center height (*h*): $h = -0.32 + 0.85 * H1$, $R^2 = 0.93$, RMSE = 0.98;
- Crown ellipticity (*b/R*), which was fixed at the mean value of the 40 field measurements: mean = 1.17, standard deviation (s.d.) = 0.46, since no significant relationship was found between *b/R* and DBH or H1.

Finally, the variations in canopy structure with stand development can be characterized by the means and standard deviations of the DBH and tree height (*H*1) for every individual tree.

2.2.2. LAI Measurements and Data Processing

Digital hemispherical photography (DHP) was the primary method for conducting regular monthly LAI measurements from 2005 until the present. From 2005 to 2006, photographs were taken by a worker every month using a CI-110 Plant Canopy Analyzer (Camas, WA, USA) to estimate the LAI. From 2007 onward; photographs were taken using a Canon EOS 40D digital camera equipped with a Nikon AF-DX 10.5 mm f/2.8 G ED fisheye lens. The camera was horizontally mounted at a fixed height of 0.2 m above the ground. The photographs were taken with automatic exposure under diffuse light conditions, typically soon before sunrise or after sunset.

In the ZH1 and FZ1 plots, measurements were taken on the 15th day of each month at five fixed locations per plot, facing in four cardinal directions. The images were processed using Gap Light Analyzer 2.0 software to calculate LAI_{DHP}. LAI_{DHP} measurements obtained with automatic exposure resulted in considerable underestimation because of underestimation of the ratio of green leaves to sky [35–39]. We used the effective LAI (LAI_e) measured by two LAI-2000 Plant Canopy Analyzers (LAI-2000, LI-COR) to correct the system bias in LAI_{DHP} data. One LAI-2000 unit was set at an open and flat area to measure diffuse sky light, and the other LAI-2000 unit was operated under the canopy at fixed locations as well as over the whole plots.

$$LAI_e = LAI_{DHP} + \varepsilon \qquad (1)$$

where ε can be considered as a systematic bias in the DHP method due to automatic exposure problems, and ε was set to 1.83 for the DHP method using the average value.

The clumping index (Ω) was measured with the Tracing Radiation and Architecture of Canopies (TRAC, Natural Resources Canada) system to convert LAI_e to true LAI (LAI_t) using the following equation:

$$LAI_t = (1 - \alpha) * LAI_e * \gamma_e / \Omega \qquad (2)$$

where the needle-to-shoot area ratio (γ_e) was set to 1.1 according to the results of the destructive sampling method described below, conducted in August 2015. The clumping index (Ω) was set to 0.8 and the value of the woody-to-total area ratio (α) was derived from the destructive samples for biomass estimation (0.2). A detailed description of the data preprocessing methods of LAI can be found in Appendix B.

2.2.3. Spectral Measurements: Leaf and Soil

Soil and leaf samples were collected from WS2 and WS3 at site 2. Current-year leaves were too short to be measured in April. Therefore, we collected current-year shoots every month during the leaf expansion period from May to August 2017 to measure the seasonal variations in LOPs. Trees were

selected from WS2 and WS3 separately to obtain branches from different age cohorts. Twenty branches were randomly selected and destructively harvested for each age group to conduct spectral measurements. Young leaves and mature leaves of 0–3 a were collected from the same branches; the leaves were carefully stored in sealed plastic bags and measured within 48 h.

Spectral measurements over the full spectral range (350–2500 nm) were carried out in the laboratory using a portable spectroradiometer (SVC HR-1024) attached to an integrating sphere (Model 1800-12S, Licor). All spectra were standardized using a barium sulfate standard and the calibrated light source supplied by Licor with the integrating sphere. We arranged 8–10 flat needles closely together for each measurement, avoiding overlaps or gaps, to obtain leaf samples that were sufficiently wide to cover the gap on integrating sphere. Wide transparent tape was used to assemble the leaf leaves on the vacuum side of the blade, which was removed from the central region to avoid any impacts on LOPs. LOPs were measured on the upper surface of the *Cunninghamia lanceolata* leaf samples. A group of leaf sample is shown in Figure A4 in Appendix A.

2.3. Remote Sensing Observations

Landsat Observations

Landsat sensors have a long history and provide data with a fine spatial resolution (30×30 m) that can effectively capture forest stands in the landscape. In addition to their ideal spatial resolution, Landsat data provide certain other advantages, such as reducing the inconsistencies in observations by always viewing from almost the same direction (nadir view) and at the same time of day. However, one of the drawbacks of Landsat data (with a 16-day revisit period) is their relatively low temporal frequency, which is exacerbated by cloud-cover [40]. We collected all available L1T Landsat TM/ETM+ images for our study site (path/row: 125/41) from 1987 to 2016, and abstracted pixel reflectance values with no cloud contamination. Given the high frequency of cloud cover in forested areas, Landsat observations over one year are insufficient to describe seasonal patterns. Therefore, all available pixel reflectance values from all years were sorted by the day of year (DOY), based on which seasonal trajectories of canopy reflectance were constructed. Landsat red and NIR band surface reflectance data were used to calculate EVI2, which takes advantage of the auto-correlative properties of surface reflectance spectra between the red and blue bands:

$$\text{EVI2} = 2.5 \frac{R_{NIR} - R_{RED}}{1 + R_{NIR} + 2.4R_{RED}} \tag{3}$$

where R_{NIR} is reflectance in the near infrared band and R_{RED} is reflectance in the red band.

3. Methods

3.1. Theoretical Foundation

Geometrical Optical Radiative Transfer (GORT) Model

The interaction between electromagnetic radiation and terrestrial plant canopies is a complex phenomenon and a key element in many RS applications. Among numerous methods for estimating the reflectance of forest canopies, the GORT model is based on the physical structure of the underlying scene. The GORT model is a hybrid of geometric optical (GO) and radiative transfer (RT) approaches for modeling canopy reflectance [41,42]. The GO model [43–45] quantifies single scattering in the canopy well and captures the fundamental properties of the canopy bidirectional reflectance distribution function (BRDF). The assumptions of the GO model are that the scene is composed of three-dimensional solid objects on a contrasting background and that the overall canopy reflectance can be modeled as a weighted sum of the spectral signatures of its individual scene components, based on their corresponding areal proportions within a pixel. The RT model is used to describe the multiple scattering within canopy elements in the GORT model, and the GO model and RT model are linked using canopy gap probabilities [46,47]. Due to the explicit

consideration of crown gaps and mutual shadowing effects, the GORT model is suitable for simulating forest canopy reflectance with varying degrees of discontinuity. The GORT model has been successfully applied to predict the fundamental features of black spruce forest canopies [42], radiation penetrating the forest canopy to the forest floor [48] and spectral temporal manifestations of forest succession [49].

In the GO model [43–45], the reflectance of a pixel is modeled as the weighted sum of the spectral signatures of four scene components: sunlit ground, sunlit crown, shaded ground and shaded crown, as illustrated below:

$$S = K_g * G + K_c * C + K_z * Z + K_t * T \tag{4}$$

where S is the average reflectance of the forest canopy inside a pixel; and K_g, K_c, K_z and K_t represent the areal proportions of the four components in the pixel; thus, K_g, K_c, K_z and K_t sum to unity. G, C, Z and T are the corresponding spectral signatures (reflectance in a given wavelength range) of the four components, as shown in Figure 2, which are functions of the proportions of incoming directional beams and diffuse solar radiation.
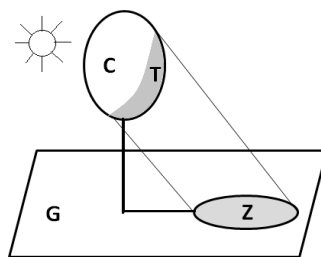

Figure 2. The four scene components used in the geometric optical (GO) model. C is the sunlit tree crown; T is the shaded tree crown; G is the sunlit background; and Z is the shaded background.

The canopy structure parameters listed in Table 1 for the stands are derived based on the field measurements of the DBH and tree height of every individual tree in the stands, and the allometric relationships between DBH or tree height. Parameter $h1$ and $h2$ must represent the structure of the dominant canopy layer. Therefore, we used the mean height minus s.d. to derive $h1$ and the mean height plus s.d. to derive $h2$. FAVD is calculated by dividing LAI by the crown volume, by treating the tree crown as an ellipsoid.

Table 1. Canopy structure parameters required for the GORT model to simulate canopy reflectance.

Symbols	Parameters	Source
	Canopy Structure Parameters	
$h1$	lower boundary of canopy center height	O [1] and CERN [2]
$h2$	upper boundary of canopy center height	O and CERN
R	horizon mean crown radius	O and CERN
b/R	crown spheroid ellipticity	1.17 (O)
λ	tree stem density (trees/ha)	CERN
FAVD	foliage area volume density (m^2/m^3)	O and CERN
k	leaf angle distribution factor	0.5 (random)
	Component Spectral Parameters	
r_L	leaf reflectance	O
t_L	leaf transmittance	O
r_G	soil/background reflectance	O
	Sun-Sensor Geometry	
SZN	sun zenith angle (°)	Time, Lon, Lat [3]
VZN	view zenith angle (°)	0
VAZ	view azimuth angle (°)	0

[1] O stands for observations from field experiments from 2015 to 2017. [2] CERN: National Ecosystem Research Network at Huitong National Research Station of Forest Ecosystem (HTF), China (http://htf.cern.ac.cn/meta/metaData). [3] Lon: Longitude; Lat: latitude.

3.2. Contribution of Component LOPs to Canopy LOPs

Different leaf-age cohorts coexist in an individual tree canopy in evergreen forests and can be classified into two major groups: new leaves and mature leaves. The LOPs of new leaves are quite different from those of mature leaves, thus, neither of them is representative of the LOPs of the whole canopy. Therefore, we need to consider the contributions of new leaves and mature leaves together to obtain the overall canopy LOPs.

3.2.1. Leaf Area Proportion of New and Mature Leaves

The first factor affecting the average canopy spectral properties is the proportion of the leaf area at different ages: the higher the proportion of the leaf area for a given age, the greater its impact on canopy optical properties. Thus, we need to consider the proportions of new leaves and mature leaves viewed by the sensor. L_{total} is the total LAI of all leaves, which consists of two parts:

$$L_{total} = L_{new} + L_{mature} \tag{5}$$

including the LAI of new leaves (L_{new}) and mature leaves (L_{mature}). The proportions of new and mature leaves were estimated based on destructive field measurements conducted by Zhongkun et al. [50], who studied the LAI of leaves at different leaf ages in Chinese fir, and we constructed the seasonally dynamic leaf area proportions by interpolating the data recorded using the phenology rule, assuming stable proportions to be reached at summer.

3.2.2. Spatial Organization of New and Mature Leaves

In addition to differences in the quantities of new and mature leaves, the spatial organization of new and mature leaves also has significant impacts on canopy component spectral signatures. Top crowns are mostly occupied by new leaves, and approximately 80% of the upper crown leaf area is occupied by new leaves in Chinese fir canopies [50]. Leaves distributed in upper crowns have significant impacts on canopy reflectance when viewed from the top of the crown. In contrast, old leaves (1 a, 2 a, 3 a) are mainly located in the inner and lower parts of tree crowns, which are less likely to be observed directly from the nadir view. Thus, contribution of new leaves located at the top of canopies cannot be ignored.

When we simulate canopy reflectance based on Landsat viewing geometry, new leaves occupy the majority of the field of view of the sensor, and solar radiation interacts with the leaves in the top layer first before reaching the lower canopy. Thus, new leaves in the upper canopy have a larger influence on canopy reflectance than mature leaves in the lower canopy. The influences of new and mature leaves on canopy LOPs are modeled as the areal-weighted averages of new and mature leaves observed by the sensors, as follows:

$$R_{ave} = w1 * R_{new} + w2 * R_{mature} \tag{6}$$

and

$$T_{ave} = w1 * T_{new} + w2 * T_{mature} \tag{7}$$

where R_{ave} and T_{ave} are the average leaf reflectance and transmittance at the canopy scale, respectively. R_{new} and R_{mature} are the reflectance of new and mature leaves, respectively. T_{new} and T_{mature} are the transmittance of new and mature leaves, respectively. Finally, the parameters of $w1$ and $w2$ are the areal weights for new and mature leaves, respectively.

Here, we model the areal weights, $w1$ and $w2$, considering both leaf-area and leaf-age impacts, as follows:

$$w1 = \frac{(1 - e^{-L_{new}})}{(1 - e^{-L_{total}})} \tag{8}$$

and

$$w2 = \frac{(1 - e^{-L_{total}}) - (1 - e^{-L_{new}})}{(1 - e^{-L_{total}})} = \frac{(e^{-L_{new}} - e^{-L_{total}})}{(1 - e^{-L_{total}})} \tag{9}$$

where $w1$ highlights the importance of new leaves in the crown in the top canopy, and the weight of mature leaves ($w2$) is estimated from the total contribution of all leaves after subtracting the occlusion effect of the new leaves.

3.3. LOPs at the Canopy Scale

LOPs at the canopy scale are a combination LOPs of both new leaves and mature leaves. At the leaf scale, LOPs are age-dependent and the LOPs of new leaves and mature leaves vary differentially. At the canopy scale, age-dependent LOPs provide a mechanism for producing seasonally varying forest albedo and changing NIR to red ratios, independent of changes in other canopy attributes. Our hypothesis is that component LOPs vary with leaf maturation, and contribute to the seasonality in canopy reflectance trajectories. In the following part, we describe methods for retrieving seasonal LOPs and examining the relationship between LOPs and canopy signals.

3.3.1. Model Sensitivity Analysis

To retrieve LOPs from Landsat observations using the GORT model, we need to obtain a comprehensive understanding of the sensitivity of model driven parameters. First, wide ranges are allowed for all parameters, and we used canopy structural measurements of young stands (stand age = 1 a) as the lower limit and canopy structural parameters of mature stands (stand age = 33 a) as the upper limit. Stem density and background reflectance were set to their true values. Since sensitivity analysis covered parameter ranges on a long temporal scale (1 a to 33 a), insensitive parameters are eliminated. Then, the remaining sensitive parameters are involved in the new sensitivity analysis with a smaller range, taking the field measurements of each parameter as prior knowledge.

The global sensitivity of the model parameters is analyzed using the extension of the Fourier amplitude sensitivity testing (EFAST) method [51]. EFAST is a variance decomposition method determining what fraction of the variance in the model output can be explained by the variation in each input parameter (i.e., partial variance). The basis of the EFAST method is a parametric transformation that can reduce multidimensional integrals over the input parametric space to one-dimensional quadratures using a search curve that scans the whole input space [52]. Scanning is conducted so that each axis of the parametric space is explored at a different frequency. Then, Fourier decomposition is used to calculate both the first-order sensitivity (the contribution to the variance of the model output by each input, S_i) and total-order sensitivity (the first-order effect plus interactions with other inputs, S_{Ti}) of each input parameter, given as (Saltelli et al., 2008):

$$S_i = \frac{V_i}{V(Y)} = \frac{V[E(Y|X_i)]}{V(Y)} \tag{10}$$

and

$$S_{Ti} = S_i + \sum_{j \neq i} S_{ij} + \ldots = \frac{E[V(Y|X_{\sim i})]}{V(Y)} \tag{11}$$

where $X_{\sim i}$ denotes the variation in all input parameters except for X_i, and S_{ij} is the contribution to the total variance from the interactions between parameters.

Following Saltelli et al. [53], to compute S_i and S_{Ti}, we created a quasi-random sequence parameter sampling matrix, P, with dimensions of (m, n) for each SA test, where m is the sample size, and n is the number of input parameters. We set $m = 2^n$, which was sufficient to test the convergence of the sensitivity index and the stability of the rankings. Each row in matrix P represents a possible value set of X, and the quasi-random sequence helps to distribute the sampling points as uniformly as possible in the parameter space and avoid clustering, in addition to increasing the convergence rate. The global sensitivity analysis method is complex, and more details can be found in the work by Saltelli [53–55]. Fortunately, SimLab software [40] can help implement the EFAST method.

3.3.2. Model Inversion Strategy

In this section, we describe the GORT model inversion strategy used to retrieve LOPs from satellite observations. Landsat reflectance in the red and NIR bands and the derived EVI2 were used to retrieve sensitive parameters. The multi-stage inversion strategy proposed by Li et al. [56] was adopted for parameter retrieval. The main objective of the iterative inversion process is to adjust the model parameters so that the model output reflectance is as close as possible to the observed reflectance. The most sensitive parameter is retrieved first, and used as prior knowledge in the next inversion stage.

One of the most popular methods for solving the inversion problem is to minimize the cost function of control variables. In this study, the cost function [57] used to retrieve sensitive parameters from Landsat surface reflectance data is as follows:

$$J(x) = \frac{1}{2}\left(\sum_{n=1}^{N} \frac{\left[f_n(X) - y_n{}^{obs} \right]^2}{\delta_n{}^2} + \sum_{l=0}^{L} \frac{\left[X_l - X_l{}^{prior} \right]^2}{\delta_l{}^2} \right) \tag{12}$$

where $y_n{}^{obs}$ and $f_n(X)$ are the observed reflectance/EVI2 value and the corresponding modeled reflectance/EVI2 value, respectively. The variables $\delta_n{}^2$ and $\delta_l{}^2$ are the variances of the observational data and the prior distribution of parameters, respectively. The variables X_l and $X_l{}^{prior}$ are the parameter values and the initial values in the model, respectively. N is the number of observations, and L is the number of parameters. Sequential quadratic programming [58], an optimization algorithm for solving nonlinear programming problems, was adopted to search for the cost function minimum.

3.3.3. Validation: Direct and Indirect Methods

During the retrieval process, the LOPs of mature leaves in the red and NIR bands were set to fixed values, except for leaf transmittance in the NIR band, which was interpolated using field measurements; the LOPs of new leaves in the red band were also interpolated using SVC measurements for leaves. The retrieval results for new leaf LOPs in the NIR band were tested in direct and indirect ways, as shown in Figure 3.
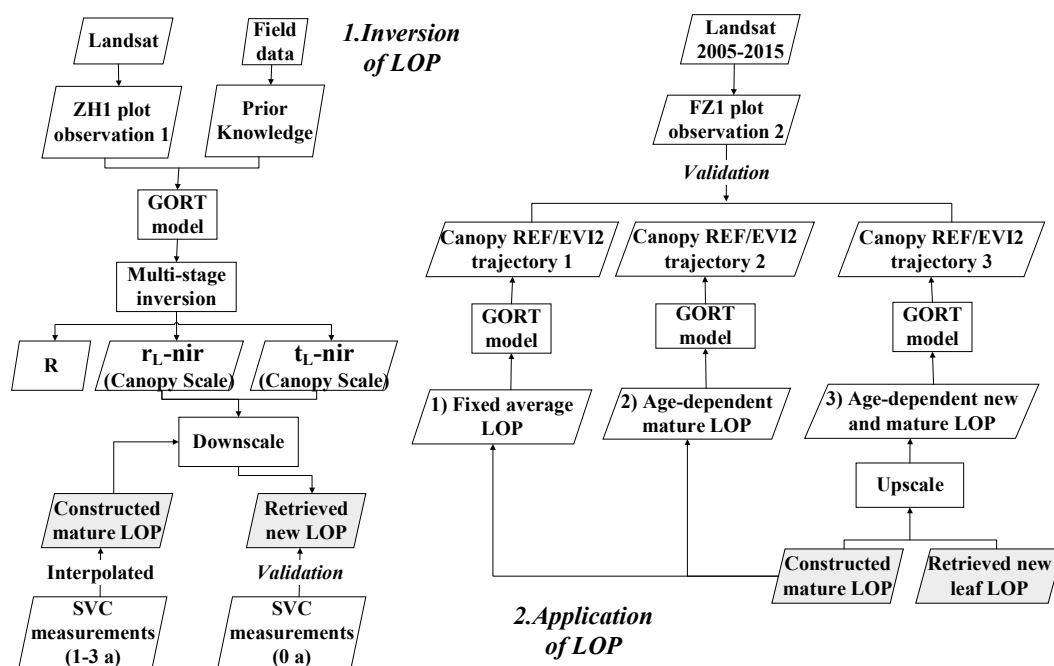

Figure 3. Flow chart of LOPs retrieval and application method.

We decomposed retrieved LOPs into new leaf (time variant) and mature leaf (known) components according to the calculated the contribution weights (*w*1 and *w*2) described in Section 3.2, and evaluated the decomposed LOPs transmittance using SVC field measurements directly. Additionally, we tested the applicability of the retrieved LOPs as a second-step validation. LOPs retrieved at one site (ZH1 plot) were applied to another site (FZ1 plot) to simulate canopy reflectance using the GORT forward simulating mode, and evaluated pixel reflectance using Landsat observations. FZ1 plot and ZH1 plot have similar growing conditions, but are located at different stands at Station 1. These sites exhibit different canopy structure properties but with the same tree species, stem density and stand age and close LAI values. In the simulation of canopy reflectance for FZ1 plot, the same LOPs, sun-sensor geometry and soil reflectance for the ZH1 plot were used, but a used different canopy structure was employed.

During the forward simulation process for canopy reflectance, three situations were considered and compared: (1) without taking leaf-age effects into consideration: setting LOPs parameters as fixed values using monthly average r_L-nir and t_L-nir of mature leaves; (2) considering the leaf-age effects for mature leaves: setting LOPs parameters using monthly varying r_L-nir and t_L-nir datasets of mature leaves; and (3) considering the leaf-age effects of both mature leaves and new leaves: setting LOPs parameters using monthly varying canopy-scale r_L-nir and t_L-nir datasets, which are up-scaled from the seasonal LOPs of new leaves and mature leaves. Finally, simulated canopy reflectance signatures were compared with pixel reflectance derived from Landsat time-series observations at FZ1 as an indirect validation.

4. Results

4.1. Sensitivity Analysis and Retrieval Results: GORT

4.1.1. Total-Order and Single-Order Sensitivity Analysis Results

Sensitivity analyses run two times for the GORT model for the red band and the NIR band. In the first sensitivity analysis, parameters with wide ranging variations were involved in the sensitivity analysis. In the second sensitivity analysis, we eliminated stem density (λ) and crown radius (*r*) in the analysis and focused on the remaining parameters, since stem density was known during our study time, and the average tree crown radius can be estimated based on the allometric relationship with DBH. In the second sensitivity analysis, the remaining parameters (LAI, *h*1, *h*2, λ, r_L, t_L, r_G) varied within the same range as in the first sensitivity analysis.

The sensitivity of the model input parameters was characterized using the total-order sensitivity index (Figure 4). For canopy reflectance in the red band, canopy reflectance is most sensitive to the crown radius and stem density in the first step of sensitivity analysis (Figure 4A). Given *r* and λ are known, LAI, *h*2, r_L and t_L become the most influential parameters in order (Figure 4B). For canopy reflectance in the NIR band, r_L, *h*2 and *r* are the main influential parameters over the long-term (Figure 4A). After removing the uncertainty of the crown radius and stem density, t_L becomes the third most influential parameter following r_L and *h*2.

To reveal the potential for retrieving uncertain parameters from canopy reflectance, we further analyzed the single-order sensitivity of each sensitive parameter in the GORT model outputs by fixing other parameters at stand average values. Taking the year of 2005 as an example, the single-order sensitivity results are shown in Figure 5. We found that during our study period, LAI and *h*2 were not influential regarding canopy spectral signatures in the red (Figure 5A) band, since LAI remains within a limited range (LAI > 3 m^2/m^2) for mature evergreen forests, and the crown radius remained the most influential parameter, especially in the red band (Figure 5A). For canopy reflectance in the NIR band, *h*2 was not influential within the range (18–23 m) for mature evergreen forests (Figure 5B). LOPs were sensitive parameters for both the red and NIR bands.
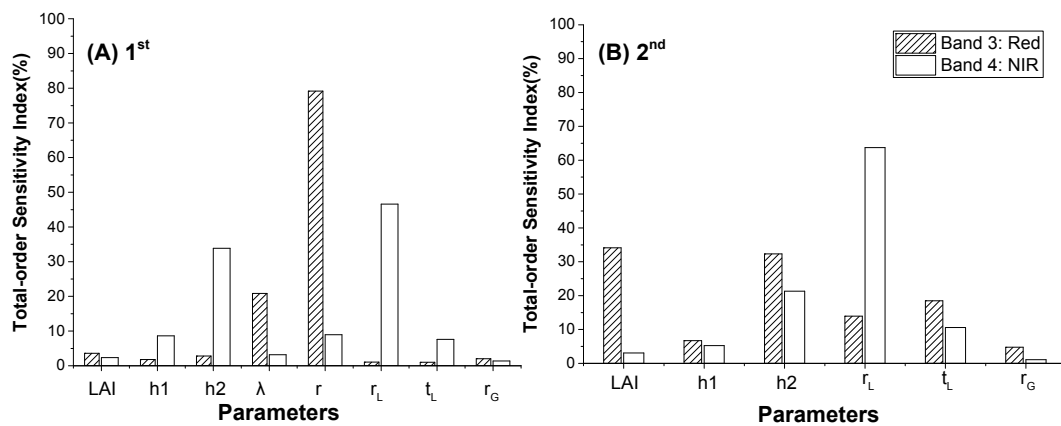
Figure 4. Results for the first (**A**) and second (**B**) global sensitivity analyses of the GORT model in the third (red) and fourth (NIR) Landsat bands for the following parameters: LAI (leaf area index), $h1$ (lower boundary of canopy center height), $h2$ (upper boundary of canopy center height), λ (tree stem density (trees/ha)), r (crown radius), r_L (leaf reflectance), t_L (leaf transmittance), and r_G (background reflectance).
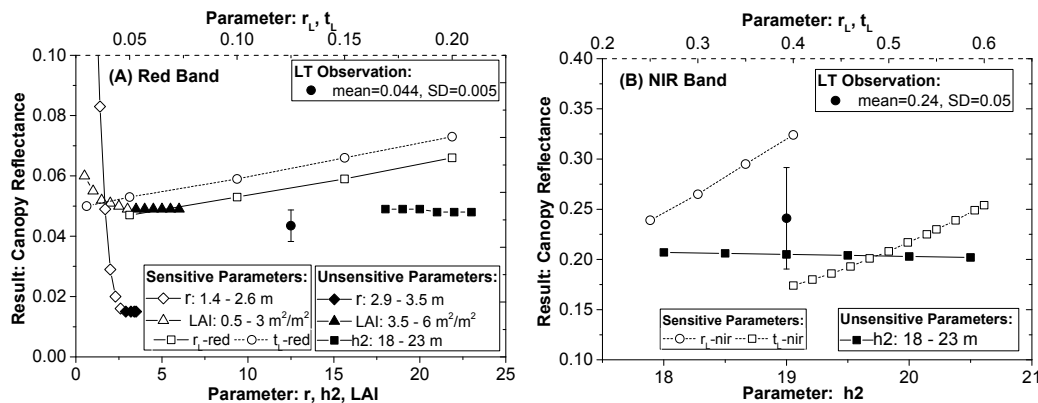

Figure 5. Single order sensitivity analysis of the impacts of sensitive parameters on GORT model outputs for the red band (**A**) and the NIR band (**B**). Only one of the model sensitive parameters was adjusted each time to study variations in the model output spectral signatures.

4.1.2. Prior Knowledge of Model Parameters

All prior knowledge of parameter values was obtained from field measurements and used for analyzing the sensitivity indexes of model parameters, as summarized in Table 2. According to total-order and first-order sensitivity analysis results, the influential parameters include: the crown radius (r), r_L and t_L, which were assumed to be adjustable during retrieval process. Non-influential parameters were set to values estimated using field measurements as described in Section 2.2. Multi-process model inversion was conducted in the following sequences: (1) Landsat red band reflectance $->$ crown radius (r); (2) Landsat NIR band reflectance/EVI2 $->$ leaf reflectance (r_L) for the NIR band; (3) Landsat NIR band reflectance/EVI2 $->$ leaf transmittance (t_L) for the NIR band; (4) Landsat red band reflectance/EVI2 $->$ leaf reflectance (r_L) for the red band; (5) Landsat red band reflectance/EVI2 $->$ leaf transmittance (t_L) for the red band. The results for the retrieved parameters are summarized in Table 2.

Table 2. Prior knowledge of input parameters and corresponding value ranges used in sensitivity analysis.

Parameter	Results	Prior Knowledge * (s.d.)	Lower Limit	Upper Limit
LAI	-	-	0.07	5.27
$h1$	-	-	1.49	13.5
$h2$	-	-	2.48	22.5
stem density (λ)	-	-	0.1035	0.252
crown radius (r) [1]	1.7	1.5	0.92	2.57
r_L-red		0.07(0.02)	0.05	0.12
t_L-red		0.04(0.03)	0.02	0.1
r_G-red	-	-	0.3	0.4
r_L-nir		0.52(0.02)	0.35	0.6
t_L-nir [1]		0.36(0.05)	0.25	0.4
r_G-nir [1]	-	-	0.35	0.45

[1] Adjustable parameters. * The prior knowledge is the initial value of parameters; the lower and upper limit values are the thresholds of the parameters.

4.2. Optical Properties of Individual New and Mature Leaves

4.2.1. Leaves at Different Ages

We first studied the leaf-age effect on leaf optical properties, and found that leaves in the canopy can be classified into two age groups: new leaves (0 a) and mature leaves (1–3 a). Field SVC measurements of the full spectra for all leaf samples were converted to Landsat-view using the Landsat relative spectral response (RSR) functions in the following three bands: green, red and NIR. Leaf samples were grouped into four age classes: 0 a, 1 a, 2 a and 3 a. Significant differences in LOPs were observed between 0 and 1 a leaves, while the differences between mature leaves at different ages (1–3 a) were not distinct (Figure 6). Thus, LOPs mainly varied within 0–1 a, i.e., during the maturation process of newly flushed leaves.
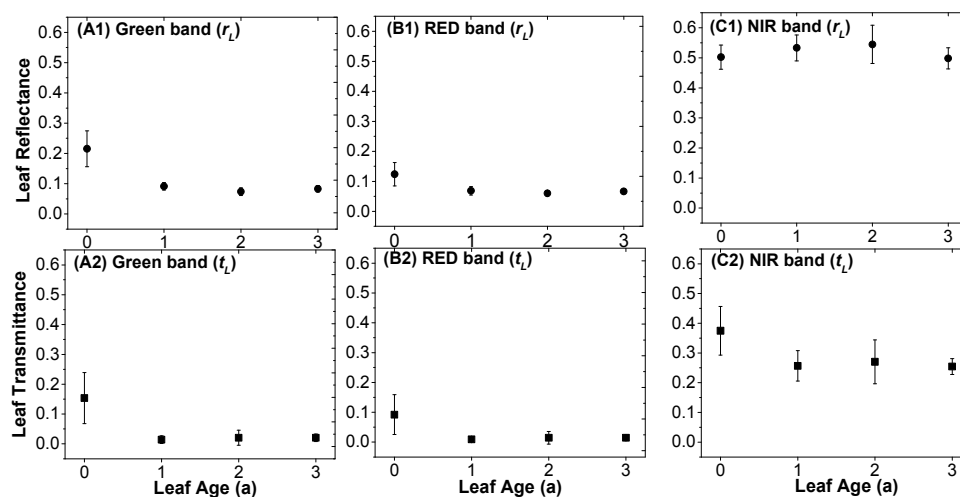

Figure 6. Leaf reflectance (r_L, **A1**–**C1**) and transmittance (t_L, **A2**–**C2**) for Chinese fir leaves at different ages (0–3 a) at three (green, red and NIR) short-wave bands. Leaves were collected on 5 May 2017.

Differences in leaf reflectance at different ages are observed in two visible bands and the NIR band (Figure 6A1–C1). New Leaves (0 a) exhibited a higher reflectance in the green and red bands compared with mature leaves (Figure 6A1–B1). In the NIR band, 1 a and 2 a leaves exhibited a slight increase in reflectance, but the reflectance of 3 a leaves was similar to that of 0 a leaves (Figure 6C1).

As can be observed in the Landsat-view transmittance signatures shown in Figure 6A2–C2, the trends in the changes in transmittance characteristics as a function of age were similar for these

three bands. Significant differences were observed between 0 a and 1 a leaves, with the 0 a leaves showing a consistently higher level of transmittance compared with mature leaves. The decrease in transmittance as a function of increasing leaf age is due to the increase in absorption characteristics after a new leaf matures, which is also supported by the increasing area between the upper and lower set of curves shown in Figure 7A1–E1.
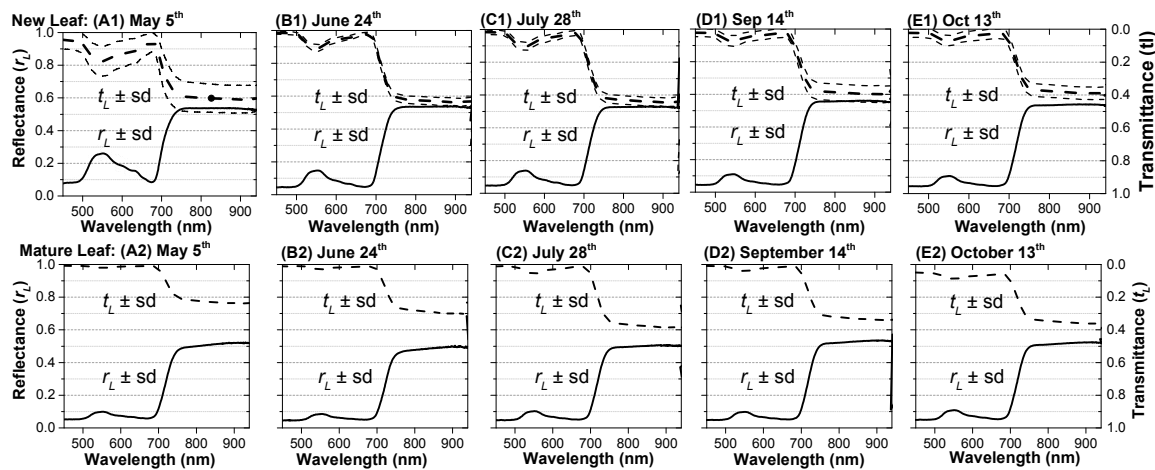

Figure 7. Field spectral curve data (mean ± 1 s.d.) in shortwave bands for new (**A1**–**E1**) and mature (**A2**–**E2**) needle samples (*n*) from Chinese fir collected on 5 May, 24 June, 28 July, 14 September and 13 October 2017. From May to October, *n* = 22, 15, 26, 30 and 39 respectively, and each sample includes 5 to 8 leaves. Reflectance data (r_L) for each month are presented as the lower set of curves within each plot, while transmittance data (t_L) are presented as the upper set of curves. Absorption characteristics are depicted based on the area between the upper and lower set of curves. SD values for new leaf t_L are depicted in the upper and lower dash lines, to avoid overlap with r_L, while SD values for all other r_L and t_L measurements are depicted in gray buffed areas.

4.2.2. Leaves in Different Seasons

The results of monthly LOPs measurements during the leaf expansion period (May to October) of 0 a leaves sampled from the Chinese fir trees are presented in Figure 7. As shown in the SVC spectral curve data for Chinese fir, significant differences were observed in the following spectral regions: the green peak (≈530–600 nm), the chlorophyll absorption well (≈660–690 nm) and along the NIR plateau (750–900 nm).

Differences in leaf reflectance are most pronounced in the green band. New leaves (0 a) exhibited a consistently lower green peak reflectance from May to October, while reflectance in the chlorophyll absorption region was shown to increase with age, especially during the first two months of the leaf expansion period, which is consistent with the increasing trend in NIR reflectance from 0 a to 1 a leaves as presented in Figure 6C1. Although this variation in NIR band reflectance is not as pronounced as in the green bands, it could have a greater impact at the canopy scale from the view of satellites, as illustrated in the following section.

With regard to leaf-level transmittance (Figure 7A1–E1), 0 a leaves showed a remarkable decrease in transmittance in the visible region from May to October, which was similar to that observed in the variations in leaf transmittance from 0 a to 1 a (Figure 7A2–B2). NIR transmittance characteristics first showed a slight increasing trend (from 1 May to 28 July) and presented a decreasing trend thereafter (from 28 July to 13 October), which coincided with the changing trend in new leaf NIR transmittance trajectory retrieved from Landsat observations (Figure 8A1). However, the observations from May to October could not fully explain the gap in the NIR transmittance of 0 a and 1 a leaves (Figure 8C2). One possible reason is that leaf transmittance decreases during winter (November to April), which may be supported by the new leaf transmittance retrieved from Landsat observations in winter time. As can

be observed in Figure 8C1, NIR transmittance decreased significantly in November and December, but there is still a gap between the retrieved new leaf transmittance (0.2) and measured leaf transmittance (0.25) at the point of reaching 1 a in May of the following year after leaf production.
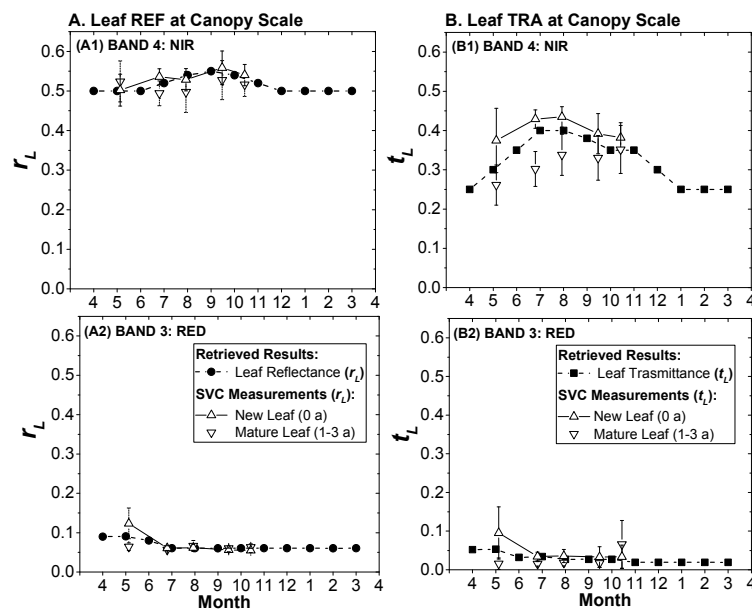

Figure 8. Retrieved results for leaf reflectance (r_L) and transmittance (t_L) at the canopy scale in the NIR band (**A1,A2**) and RED band (**B1,B2**).

4.3. Leaf-Age Effects on Variability in Landsat-Viewed Canopy Reflectance

Landsat records canopy LOPs from the sensor view and time-series data can be used to estimate seasonal variations in LOPs. First, we attempted to retrieve LOPs at the canopy scale from Landsat observations using the GORT model. Then, we estimated the new leaf component from the retrieved results by setting mature leaf component parameters as known parameters using field measurements. The results were evaluated via direct and indirect methods.

4.3.1. Leaf Optical Properties at the Canopy Scale

After considering the uncertainties and sensitivities of other parameters in the GORT model, seasonal LOPs were retrieved from Landsat observations using the proposed multi-stage inversion method by minimizing the cost function. Retrieved LOPs at the canopy scale are shown in Figure 8 and compared with field measurements of the spectral signatures of leaves. Changes in Landsat reflectance were associated with variations in leaf optical properties. As shown in Figure 8A1–B1, the most dramatic changes occurred in the NIR band, resulting in increased reflectance and transmittance during spring (April to September) and decreased reflectance and transmittance during winter (October to December). However, variations in NIR reflectance (0.5 to 0.55) were less notable than that of NIR transmittance (0.25 to 0.4). In the red band (Figure 8A2–B2), differences in LOPs mainly occurred in the first three months (May to July) and then became stable in the rest of the year. Both red reflectance and transmittance presented low values, and transmittance was slightly lower than reflectance. No LOPs changes in red band could be observed from Landsat alone, but including EVI2 data helped to some extent.

4.3.2. Seasonal Leaf Optical Properties

When viewed from the top of the crown, LOPs retrieved from Landsat observations are a combination of leaves of all ages. As analyzed in Section 3.3, we account for both the effects of

leaf area and its spatial organization in the canopy to estimate the contribution of different leaves. Figure 9 shows the average seasonal variations in total leaf area (A) and leaf proportions (B) of new leaves and mature leaves in the canopy, and their contributions to canopy spectral properties (C). The time period starts at leaf expansion at age 0 (April) and ends with leaf maturity (March in the following year) at age 1, following the same twelve-month cycle with new leaf expansion each year. We can see that LAI does not change very dramatically for evergreen forests between seasons in our study period (Figure 9A). Thus, the satellite-observed seasonality of canopy reflectance is not determined by LAI, but rather is the result of variations in the LOPs of new leaves during the maturation process. Although new leaves only account for approximately 30% of the total leaf area (Figure 9B), new leaves made high contribution (approximately 80% at the peak time in summer) to canopy spectral properties from the crown top view (Figure 9C).
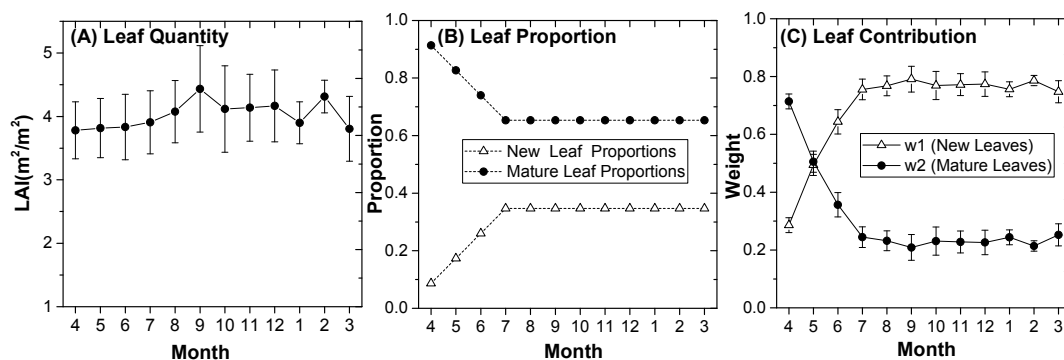

Figure 9. Seasonal variations in the leaf properties of the canopy, including (**A**) total leaf area: average LAI from stand age 22 to 33 (2005 to 2015); (**B**) leaf proportion: the percentage of new leaves and mature leaves in the canopy measured by Zhongkun et al. [50]; (**C**) weights for new leaves ($w1$) and mature leaves ($w2$) from stand age 22 to 33 (2005 to 2015).

The seasonal trajectories of mature leaf LOPs (Figure 10 B1,B2) were interpolated from field measurements, which were quite stable during growing season, with only one exception: NIR transmittance. Mature leaf transmittance in the NIR increased by 30% over the three months following the beginning of a new growing cycle in May (Figure 10B1), while mature leaves showed no significant difference in NIR reflectance during the whole growing season (May to November).

New leaf reflectance or transmittance can be estimated by deducting the contribution of mature leaves from the retrieved LOPs results, which are shown in Figure 10. It can be seen that the retrieved new leaf LOPs were in good agreement with the field observations (Figure 10A1,A2) from May to October. We can also see that new leaf LOPs in the red band decreased in the first three months (from April to June) and became stable thereafter (Figure 10A2). More importantly, new leaf NIR REF continued to increase from May to September after production (approximately 11%), while new leaf NIR TRA follow a nonlinear trajectory, increasing from May to August (approximately 16%) and decreasing thereafter (approximately 14%). A small increase in new leaf NIR REF and a small decrease in new leaf NIR TRA could both translate into a larger impact at the canopy scale, when the canopy is coated with new leaves, and the impact of the leaf-age effect at the canopy scale will be further studied in the following section.

A gap exists between the estimated new leaf NIR transmittance and SVC measurements in May, and the s.d. values of new leaf field measurements in May are greater than the measurements in other months (Figure 10A1,A2). This might be explained by the overestimation of measured leaf transmittance samples when leaves were small, which was caused by unavoidable small gaps because of minor misalignment in the arrangement of leaves. Large s.d. values for new leaf field measurements in May could also occur due to the differences in leaf expansion rate and maturity times in the early leaf flush period.
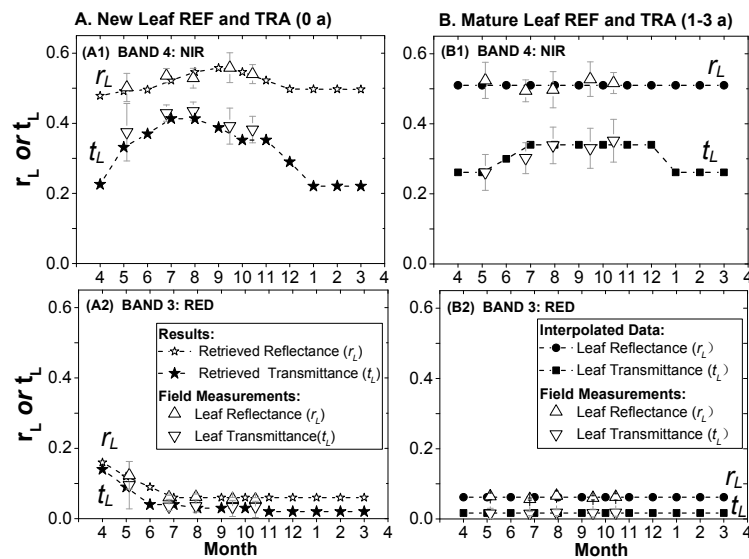
Figure 10. Validation of estimated new leaf LOPs in the NIR band (**A1**) and red band (**A2**) and the constructed mature leaf LOPs trajectories (**B1,B2**).

4.3.3. Leaf-Age Effects at Pixel Scale Based on Satellite Observations

LAI and sun-sensor geometry are widely recognized as the main factors contributing to seasonality in RS signals [12,19]. Thus, we need to distinguish leaf-age effects from the contributions of these two factors. To identify the contribution of leaf-age effects to the seasonality in Landsat signals, we compared the differences in the results with/without considering leaf-age effects. The forward-mode GORT model was used to simulate canopy reflectance at the pixel scale with Landsat-viewing geometry, and the model-driven parameters are listed in Table 1. We simulate canopy reflectance at NIR band and red band in the following three circumstances:

1. In the first circumstance, we ignore the leaf-age effects caused by aging mature leaves and growing new leaves, and only consider variations in LAI and sun geometry using field data. LOPs in the GORT model were fixed using the mean LOPs for mature leaves measured from May to September in 2017 (NIR band: $REF_{mature} = 0.51$, $TRA_{mature} = 0.26$ or 0.34; Red band: $REF_{mature} = 0.06$, $TRA_{mature} = 0.01$).

2. Based on circumstance 1, we include variations in LOPs caused by aging mature leaves. For comparative purposes, we first added variations in mature leaves using data shown in Figure 10B1 to drive the GORT model.

3. Based on circumstance 2, we further include variations in LOPs caused by production and expansion of new leaves. LOPs for the GORT model are shown in Figure 8B1. LOPs at the canopy scale retrieved at the ZH1 site are applied to the FZ1 site with different canopy structure parameters.

The overall GORT-simulated results obtained for the three circumstances are compared in Figure 11. After considering the mature leaf-age effects on canopy reflectance, the R^2 between the simulated canopy reflectance/EVI2 and the Landsat observations increased significantly (from 0.38 to 0.83 for canopy NIR reflectance and from 0.26 to 0.43 for canopy EVI2), as shown in Figure 11. However, the R^2 of both groups in the GORT simulation results was poor in the red band and RMSE remained low.

In circumstance 1, we can see that LAI is stable (Figure 9A) in these sub-tropical forests and is not the main factor contributing to the seasonality of canopy NIR REF. Seasonal variation in sun-sensor geometry from January to June to December (SZN varies from 56° to 25° to 56°) causes a small amount of seasonality of forest albedo, as shown based on the blue line in Figure 11A1. However, SZN alone does not sufficiently explain the seasonality of the Landsat canopy signals in our study sites. Assuming that the LOPs of mature leaves do not change, if we apply mature leaf LOPs measured at the peak time in summer (NIR TRA = 0.34)

to other times, we might overestimate canopy NIR REF in winter; and if we apply mature leaf LOPs measured in early spring (NIR TRA = 0.26), we might underestimate canopy NIR REF in summer.

In circumstance 2, we consider the leaf-aging effects of the mature leaves, which constitute the majority (>60%) of the canopy LAI (Figure 9B). The LOPs of mature leaves are relatively stable in the red and NIR bands, therefore, mature leaves have no impact on canopy red REF. However, there is one notable exception: mature leaf NIR TRA is lower in winter and greater in summer and continued to increase from May to October (Figure 7A2–E2). The winter-summer differences in leaf NIR TRA contribute to a steeper NIR REF/EVI2 trajectory from April to July at the canopy scale, as shown based on the area between the blue and gray curves in Figure 11A1,C1.

In circumstance 3, we can observe how variations in the LOPs of new leaves contributed to the seasonal variation in canopy NIR reflectance and derived EVI2 (Figure 11A1,C1). As shown based on the area between the green and gray curves in Figure 11A1,C1, EVI2 trajectories follow the same pattern (Figure 11C1) as NIR reflectance. In general, new leaf production and expansion increases canopy NIR reflectance from May to October (Figure 11A1). An increased new leaf TRA (18%) also contributes to the increase in NIR REF at the canopy scale, but only before August. After September, an increase in NIR REF is caused by an increase in leaf REF. However, the changing trend of canopy NIR REF is nonlinear, which increases from May to August and decreases from August to October. As illustrated in Figure 10A1, canopy NIR REF increases from May to August partially due to increasing new leaf NIR REF during this period; conversely, canopy NIR REF decreases from August to October due to decreasing new leaf TRA at this interval.

The upper-layer-located new leaves provide a mechanism for producing greater seasonality of forest albedo in addition to mature leaves. A small increase in new leaf NIR REF (0.05 unit) has significant impacts at the canopy scale, since new leaves are generally located at the top of the canopy. New leaf expansion also contributes to negligible increase in canopy Red REF from March to July (Figure 11B1). EVI2 trajectories follow the same patterns (Figure 11C1) as NIR reflectance trajectories, arising from the linear dependence of EVI2 on NIR reflectance, as proved by a previous study [23]. We can conclude that both new and mature leaves contribute to the seasonality of forest albedo, which is independent of changes in other canopy attributes.
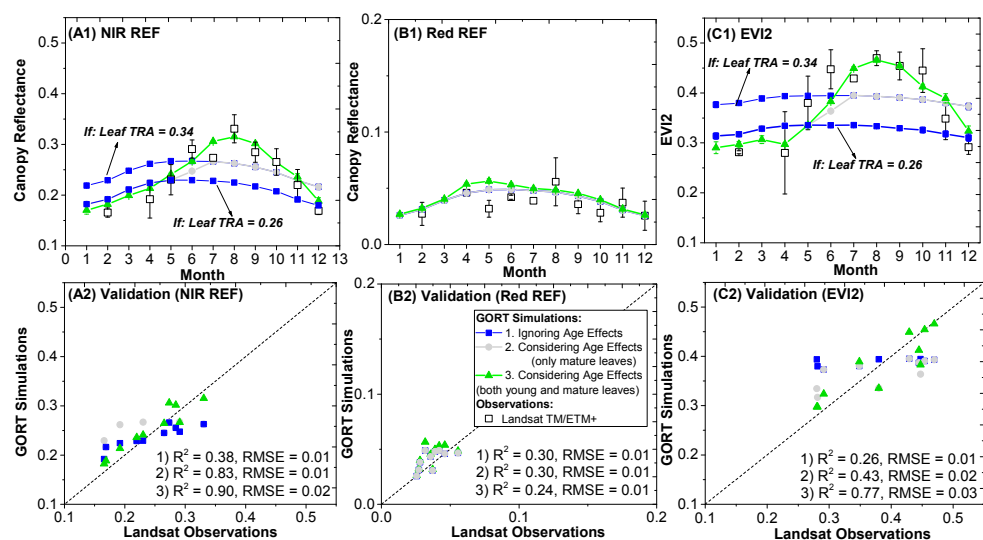

Figure 11. Aging effects of new leaves and mature leaves on seasonality of canopy signal trajectory in NIR band (**A1**), red band (**B1**) and EVI2 (**C1**). With the exception of the differences in leaf optical parameters, all other input parameters for the GORT model are the same in three circumstances. We evaluated the simulated canopy signature with Landsat observations (**A2–C2**). Both the simulated results and Landsat observations are at a monthly step with the mean value and s.d. (from 2005 to 2015).

5. Discussion

5.1. Spectral Changes and Leaf Aging

For Chinese fir, the leaf spectra mainly vary during the first year of leaf production (0–1 a), and then remain relatively stable from 1–3 a. During the new leaf expansion process, leaf water content (LWC) and the specific leaf area (SLA) decrease rapidly, resulting in variations in LOPs: including decreased transmittance and increased absorbance in the visible and NIR bands and decreased visible, but increased NIR reflectance. Leaf optical properties show strong age dependence and great seasonal difference for young and mature leaves. Spectral changes in the visible portion of the spectrum characterized the new leaves while increased NIR transmittance and decreased NIR absorbance characterized mature leaves. Changes observed in the visible spectrum matched similar observations for Carica [59] and Aldina [60]. In general, absorbance at the green peak (550 nm) increases, while reflectance and transmittance decrease at this band, which could be attributed to an increase in chlorophyll [59] and changes in leaf internal anatomy [61]. However, the changes of LOPs in the NIR band are complicated.

In agreement with previous findings [60], mature leaves were found to show a lower leaf albedo (leaf reflectance plus transmittance) at the NIR band than new leaves due to leaf aging. Early changes in the NIR band were noted during new leaf expansion, with a slight increase (11%) in leaf NIR REF being observed from May to October and a continuous increase (14%) in leaf TRA being recorded from May to August, followed by a slight decrease in NIR TRA during autumn and winter. Some studies [62] have found a dramatic increase in leaf NIR reflectance between July and August, which might be caused by differences in the leaf characteristics. Low-wax leaves display a continuous increase in NIR reflectance until maturity, while high-wax leaves show little increase in NIR reflectance [63]. Epicuticular waxes and thick cuticles could mask the effect of NIR increases caused by inter-cellular development in young high-wax leaves. These characteristics might explain why only a slight increase in NIR reflectance was found during leaf maturation in the present study, since Chinese fir is a high-wax species.

In contrast to previous studies, we observed a continuous increase in NIR transmittance for mature leaves (1–3 a). However, a significant gap in NIR transmittance existed between new leaves (measured from May to October) and mature leave (measured in May), and we only observed a small decrease in NIR transmittance for new leaves from September to October. However, a dramatic decrease in NIR transmittance might happen in winter time (November to December to January) according to the results retrieved from Landsat observations, which will be further studied in the future. Similar observations have been made by others [60], who found a consistent decrease in NIR transmittance during the last nine months of the leaf cycle.

5.2. Leaf-Aging Effects on Canopy Reflectance

At the canopy scale, canopy reflectance is a product of competing mechanisms of light absorption [60]. The interaction of photons with dense forests is characterized by strong scattering in the NIR and equally strong absorption in the shorter red and blue bands. The NIR reflectance of these forests is an order of magnitude greater than the reflectance at red (blue) band. On the other hand, aerosol scattering has greater impacts on reflectance in visible bands than the NIR band. In the NIR band, any mechanism that increases leaf absorption (such as decreased transmittance or reflectance) will have an enhanced effect on canopy reflectance [60]. Thus, we could expect leaf aging to have its largest impact in the NIR band.

Age-related LOPs are factors that require special attention but have been overlooked in previous studies focused on estimating vegetation status using optical signal trajectories. Previous studies also found changes in canopy NIR reflectance caused by the exchange of older leaves for newer leaves [23,24,27]. These studies considered the differences in LOPs between senesced old leaves and new leaves, but they ignored the simultaneous aging process of new leaves and mature leaves with a life span of more than three years. In this study, the observed seasonality of the canopy NIR reflectance of

evergreen forests was due to age-dependent leaf optical properties at the NIR band, including both new leaf maturation and mature leaf aging, with little changes in total leaf area. New leaf maturation mainly increases NIR reflectance at the peak time in summer (May to October), and mature leaf aging mainly reduces NIR reflectance during early spring (January to June). We have already excluded differences caused by changes in the solar zenith angle [10], and our seasonally moist sub-tropical forests are free of drought impact [24,64–66] or the impact of epiphylls on mature leaves in tropical forests [23,60,67], which are highly debated factors causing changes in NIR reflectance in numerous studies, and the same seasonality pattern is observed in EVI because of its strong dependence on NIR reflectance.

It is important to note that the forest canopy is composed of mixed-age leaves. Mature leaves account for a major population, while a higher proportion of young leaves are observed by the Landsat satellite because of their distribution at the top of the canopy. Both new and mature leaves influence canopy NIR reflectance, and their impacts change with new leaf expansion. New leaf expansion changes the proportions of young and mature leaves within a forest canopy over the season, thus, further changes the canopy spectral signatures.

5.3. Potential Implications for Photosynthesis

Young leaves exhibit a higher photosynthetic capacity than older leaves, and it is therefore essential to track changes in the age-structure of leaves in the canopy, which could substantially improve the modeling of the seasonal dynamics of photosynthesis. Xiaoquan and Deying [68] studied the leaf-age effects on the photosynthetic characteristics of 18-year-old *Cunninghamia lanceolata* stands and found similar trends in leaf photosynthetic rate at different ages: the photosynthesis rate of newly flushed leaves increases during the maturation process and then decreases at the end of the growing season, while the photosynthesis rate of mature leaves (1 and 2 a) decreases as time progresses. This study suggested that considering the temporal variation in the LOPs of new leaves matters significantly in understanding the seasonal trend of canopy spectral signatures. Ignoring variations in leaf-scale properties may mislead our interpretations of seasonality of RS signals from evergreen forests where different-age leaf cohorts coexist in the canopy. This study provides new evidence of the importance of considering the phenology of LOPs at different ages and which could contribute to more accurately modeling of photosynthesis [69].

5.4. Implications of LOPs and Canopy Structure

At the canopy scale, seasonal variations in new leaf optical properties were shown to be the dominant factor producing seasonal variations in canopy reflectance and altering NIR to red ratios, independent of changes in other canopy attributes. However, our study explicitly focused on dense evergreen forests with stable LAI (LAI > 3). The parameters that drive the GORT model may vary on different temporal scales. For example, crown size and tree height vary annually, while LAI, leaf spectra, and sun geometry vary seasonally. We can explore the signal differences caused by LAI and canopy structure by comparing the annual differences in the GORT model outputs. We only applied the annual structural parameters from 2005 to 2015 (there were no data in 2009 and from 2012 to 2014) to drive the the GORT model. In addition to annual stable structural parameters, the SZN, LAI and canopy average LOPs were updated monthly. Although the LAI seasonality and structure parameters varied from year to year, NIR reflectance showed similar seasonal trajectories with little annual difference, as illustrated by the vertical error bar in Figure 11. There may be two explanations for this limited variation. First, there is a lack of LAI seasonality or the canopy is too dense with a high LAI; thus, small changes in leaf area are not as sensitive compared with the variations in LOPs. The results might be different for young stands, especially before canopy closure. Second, canopy structural parameters do not change significantly during the new leaf maturation process; thus, canopy structures have limited impacts on canopy reflectance during this period. As illustrated in other studies [23], LAI is also an important factor contributing to the seasonality of NIR reflectance.

This study quantified the effects of leaf age on canopy reflectance in mature evergreen forests to first explore the possible impacts on leaf quality when total leaf area does not exhibit significant seasonal

changes. Given the findings of this case study, future studies in deciduous forests, where seasonal variations in LAI are more significant and leaf-age groups are less complicated, would allow further validating of our findings and apply our findings to better quantify the canopy spectral signatures to understand the role of forests in terrestrial ecosystems.

6. Conclusions

This study evaluated the effect of LOPs for leaves at different ages on the canopy spectral signature variation during the growing season for Chinese fir stands. For closed canopy evergreen stands with relatively stable LAI, new leaves exerted disproportional influence on the canopy season spectral signature due to the spatial distribution of the new leaves in the top and outer canopy. The most direct implications of our results are related to ecological or physiological studies that utilize remote sensing, and our findings provide a promising potential to improve the interpretation of RS signals. The most significant finding of this study at the leaf scale is the increase in the NIR transmittance of mature leaves and the increase in the NIR reflectance of new leaves. To date, most of the identified contributions of leaf age to the variation in leaf optical properties have involved changes in the differences between old leaves and new leaves. Simultaneous monitoring of new and mature LOPs with season, however, has not been previously documented. In this study, we observed an approximately 11% increase in NIR reflectance (0.05 unit) for new leaves and a 35% increase in NIR transmittance for mature leaves during the growing season.

Variations of LOPs at the leaf scale have significant impacts at the canopy scale, and contribute to seasonality of canopy NIR reflectance and EVI2. Due to the complexity of forest ecosystems, analyses based on field data alone cannot provide guidance in the interpretation of RS signals. Conversely, studies based on modeling alone, without proper ground measurements of the key factors driving canopy signal variation, can be misleading. This study combined field observations with the GORT model to elucidate the effects of leaf age on canopy-scale reflectance signals. We demonstrated that, in addition to sun-sensor geometry, the effects of leaf aging on LOPs were the major factor contributing to the seasonality of canopy reflectance for the Chinese fir stands:

- New leaf maturation is the main factor contributing to seasonality of canopy signals (NIR REF and EVI2), because of the distribution of these leaves in the top and outer canopy, as well as their increasing proportions with leaf growth. A small increase (0.05 unit) in new leaf NIR reflectance results in a significant increase in canopy NIR reflectance from spring to summer, while a decrease in new leaf NIR transmittance from August to October causes a decreasing trend in canopy NIR reflectance in autumn and winter.

- Mature leaf aging is another factor contributing to the seasonality of the canopy signals (NIR REF and EVI2) because of the significant proportion of mature leaves in the canopy. Mature leaf NIR transmittance is greater during the growing season than off the growing season. This difference in leaf TRA causes an increased difference in canopy reflectance between winter and summer.

Thus, the effects of leaf age cannot be ignored when conducting time series analyses using RS data for the evergreen needle leaf forests.

Author Contributions: Q.W. and J.S. conceived and designed the experiments; C.S. and J.W. contributed to the conception of the study; S.C. and B.Y. performed the experiments; Q.W. analyzed the data and wrote the paper. C.S., J.S. and J.W. have reviewed and edited the manuscript.

Conflicts of Interest: The authors declare no conflict of interest.

Appendix A

Appendix A.1 Data Description

Section 2.2.1 is supported with field data collected for Chinese fir forest stands located in the vicinity of the permanent ecosystem research stations in National Research Stations of Forest Ecosystems in Huitong county, Hunan province, southern China. This appendix provides details on data acquisition of canopy structure parameters.

Appendix A.2 Canopy Structural Parameter Measurements

Crown shape measurements were taken for a total of forty trees in study Site 2. Measured crown shape parameters are shown in Figure A1, among which, DBH was measured using diameter tapes, and crown radius and tree heights were measured using telemeter rods. The size of the selected trees was evenly distributed uniformly in terms of height (*H*) (from 5.4 m to 20 m) and diameter at breast height (DBH) (from 7.7 cm to 37.8 cm). Among the 40 trees, 7 are located at plots close to the study site, and 33 are located within the ZH1 and FZ1 sites. The parameters measured for characterizing crown shape are presented in Figure A1, including crown width in the north-south direction (*R*1) and the east-west direction (*R*2), tree height (*H*1) and height under crown (*H*2), from which we can obtain the height of crown center (*h*). We used the measurements of these 40 trees to build regression relationships for crown width, DBH, h and tree height. Figures A2 and A3 illustrated the field measurements of canopy structure parameters as well as their growth trajectories with DBH, which usually correlates well with tree ages.
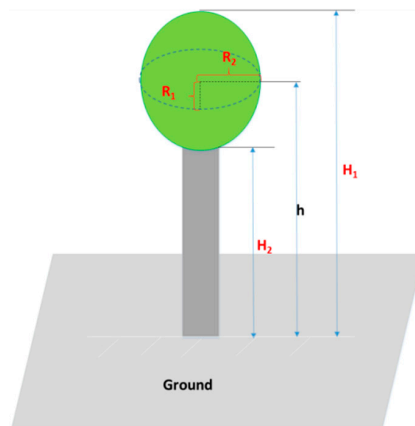

Figure A1. Measured parameters for sample trees selected to build regression relationships for the structural parameters of the tree crown and other measures, including tree height and DBH.
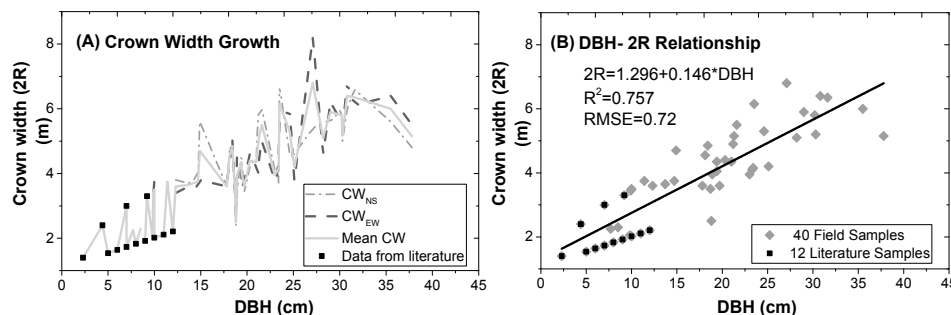

Figure A2. (**A**) Measured crown width (*2R*) for 40 sample trees with DBH in the north-south direction (CW$_{NS}$) and east-west direction (CW$_{EW}$); (**B**) Regression relationships between DBH and crown width (*2R*).
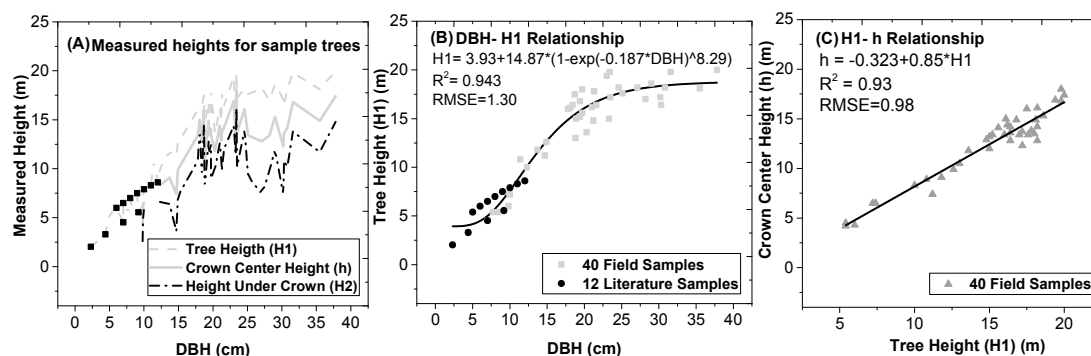
Figure A3. (**A**) Measured height values for 40 sample trees with increasing DBH. The measured data include tree height (*H1*), height of crown center (*h*) and height under crown (*H2*); Regression relationships between DBH and tree height (**B**) and between tree height and crown center height (**C**).

Appendix A.3 Leaf Area Proportion and Distribution in Crown

Table A1. Leaf area and proportion of leaves at different ages located at different crown positions for *Cunninghamia* trees in Hunan.

Leaf Age/Location	Bottom Crown	Central Crown	Upper Crown	Leaf Area ∑ (%)
0 a	1.16	1.41	3.24	5.8 (34.63%)
1 a	1.93	2.93	0.81	5.67 (33.85%)
2 a	1.80	1.59	0	3.39 (20.24%)
3 a	1.11	0.76	0	1.87 (11.64%)
Leaf Area ∑ (%)	6.00 (35.8%)	6.69 (40%)	4.05 (24.2%)	16.75 (100%)

Table origin: [50].

Appendix A.4 Leaf Sample for SVC Measurements

Figure A4. The vacuum side of one group of leaf leaves prepared for spectral measurement. Leaf samples were collected on 15 July 2016.

Appendix B

Appendix B.1 Data Description

Section 2.2.2 is supported with LAI field data collected for Chinese fir forest stands located close to the permanent ecosystem research stations in National Research Stations of Forest Ecosystems in Huitong county, Hunan province, southern China. Long-term LAI were measured monthly to drive the GORT model from year 2005 to 2015. In this time period, two different DHP methods were applied

before and after year 2006. This appendix provides details on LAI data acquisition and processing to produce consistent LAI time-series.

Appendix B.2 Long-Term LAI_e Observations: DHP Methods

(1)　2005 and 2006: CI-110 Plant Canopy Analyzer

　　Plant canopy imaging was the primary method for conducting regular monthly LAI measurements from 2005 until present. From 2005 to 2006, pictures were taken every month by one worker using a CI-110 Plant Canopy Analyzer to estimate the LAI. From 2007 onward, photographs were taken by another fixed worker using a Canon EOS 40D digital camera equipped with a Nikon AF-DX 10.5 mm f/2.8 G ED fisheye convertor. The data measured before 2007 needed to be further preprocessed prior to further calculations to make them consistent with data measured after 2007. We have 30 pairs of data measured at the same positions and in the same directions in ZH1 and FZ1 to unify the original LAI time series data using data measured in December 2006 and January 2007. We employed two methods to unify these datasets: (1) Regression Method: The first method involves deriving two average seasonal LAI trajectories, one before 2007 and the other after 2007, and calculating their regression equations. (2) Lifting Method: The second method involves acquiring the mean absolute deviation (ΔLAI = 1.01) of the data before 2007 and those after 2007 using the mean difference between these 30 pairs of LAI data. The results of these two methods are different, and both are illustrated at the end of this section.

(2)　2007 to 2015: Fisheye Digital Camera

　　From 2007 afterwards, photographs were taken using a Canon EOS 40D digital camera equipped with a Nikon AF-DX 10.5 mm f/2.8G ED fisheye convertor. The camera was horizontally mounted at a fixed height of 0.2 m above the ground. The photographs were taken with automatic exposure under diffuse light conditions, typically soon after sunrise or immediately before sunset. In the ZH1 and FZ1 plots, measurements were taken for three layers: the herb layer, shrub layer and tree layer on the 15th day of each month at five fixed locations per plot and facing toward four cardinal directions. All measurements were made under diffuse light conditions to avoid introducing errors due to the presence of sunlit foliage. The images were processed by the Gap Light Analyzer 2.0 software to calculate LAI_{DHP}.

　　Incorrect exposure has been shown to cause significant underestimations in LAI_{DHP} measurements [35–39]. All DHP measurements were taken with automatic exposures, which resulted in considerable underestimation. The LAI measurements made using the DHP and LAI-2000 methods were shown to be significantly correlated in any zenith angle range. Therefore, we calibrated LAI_{DHP} by the LAI_e measured using an LAI-2000 plant analyzer, to quantify the systematic bias ε in DHP methods due to automatic exposure problems.

Appendix B.3 Converting LAI_e to LAI_t: LAI-2000 and TRAC Methods

　　LAI-2000 and TRAC measurements were used to convert LAI_{DHP} to true LAI. Tracing Radiation and Architecture of Canopies (TRAC, Natural Resources Canada, Canada Center for Remote Sensing, Saint-Hubert, QC, Canada) and an LAI-2000 Plant Canopy Analyzer (LAI-2000, LI-COR Inc, Lincoln, NE, USA) [41] were used to measure the LAI of each sample plot [42]. The LAI-2000 was used to measure the effective LAI (LAI_e), and TRAC was used to measure both the effective LAI (LAI_e) and the foliage clumping index (Ω).

　　The LAI-2000 method is based on the measurement of diffuse radiation attenuation in the blue band caused by the canopy, which is related to gap fraction. Further details on the theories and measurements behind LAI are given in Frazer et al. [70]. We employed two LAI-2000 units to measure the sky radiation and under-canopy radiation simultaneously. Additionally, we cross-calibrated these two LAI-2000 units before the field survey. One LAI-2000 unit is horizontally mounted on a

rooftop facing toward our study sites and automatically records the above-canopy radiation every 5 min. Ninety-degree view caps were used on both units to avoid the influence of other objects on the sensors and made these measurements comparable with those from the DHP methods in four cardinal directions. The LAI-2000 measurements were taken under diffuse sky conditions in the early morning or after sunset. The TRAC method requires direct solar radiation, so we took TRAC measurements during midday at a constant walking pace along several parallel transects, which were perpendicular to the direction of tree stem shadows. Distance markers were registered every 5 m. The TRAC data were processed by TracWin software, which calculates LAI_e and the clumping index (Ω).

During August 2015, we used LAI-2000 instruments to measure the LAI in the WS2 and WS3 plots. We revisited these plots in June 2016, taking measurements with both the TRAC and LAI-2000 instruments. In June 2016, we surveyed the ZH1 and FZ1 sample plots and used the LAI-2000 instruments to measure the LAI at the same locations as measured by the long-term DHP methods. In comparison to the LAI-2000 instrument, the accuracy of DHP is affected by photograph exposure settings because these settings impact the ratio of green leaves to sky. An LAI-2000 unit was operated subsequently at the same locations for comparison with DHP, and then we convert LAI_e to true LAI values.

Additional correction parameters were required to convert LAI_e to LAI_t. The needle-to-shoot area ratio (γ_e) was measured using destructive sampling conducted in August 2015. The clumping index Ω was measured by the TRAC instrument. Additionally, the woody-to-total area ratio (α) for *Cunninghamia lanceolata* was derived from destructive sampling used to calculate biomass.

*Appendix B.4 Unifying LAI Measurements Using Different Methods*

LAI_{DHP} was corrected using LAI_e measurements from the LAI-2000 units to decrease the underestimation caused by the automatic exposure problem present in the DHP method. We made comparisons between the LAI as measured using DHP and LAI-2000 in the same locations in ZH1 and FZ1 to estimate the system bias (ε) of DHP. We applied a fixed bias instead of a regression relationship between DHP and LAI-2000 because our study site is pure *Cunninghamia lanceolata* plantations and the LAI values fall within a small range. Thus, it is not possible to build a robust regression relationship with limited LAI variations using the field measurements made on our study sites. Although previous studies have built and applied regression relationships between DHP and LAI-2000 LAI methods [71], we chose to estimate the system error of DHP with a fixed value in our study site. The reasons for this choice are listed as follows: first, regression relationships are usually site specific, lack universality and cannot be applied to other places. We used the existing regression relationship to our study sites, but the result was of poor quality. The regression relationship built by [71] resulted in a mean absolute error of 1.0 LAI when compared with field LAI-2000 measurements. Second, the accuracy of the regression relationship may vary in different ranges of values. For example, if the regression relationship fits well in the low-value range but fits poorly at high values, then when we apply it to other places with mainly high values, the relationship will fail. At this study site, the LAI is quite stable; as shown in Table A2, the standard deviation is quite small (approximately 0.25 as measured by LAI-2000), and the maximum and minimum LAI-2000 measurements within our study sites are quite close (3.19–3.36 for ZH1, and 3.18–3.3 for FZ1). Thus, correcting for the systematic error is a sufficient and reliable method for converting LAI values measured by the DHP method to LAI measured with LAI-2000.

Table A2. Comparison of effective LAI derived from digital hemispherical photography (DHP) and LAI-2000 methods.

Plot	ZH1			FZ1		
	DHP (5 pts * 4 Dirs)	LAI-2000 (5 pts * 4 Dirs)	LAI-2000 (26 pts * 2 Repeat)	DHP (5 pts * 4 Dirs)	LAI-2000 (5 pts * 4 dirs)	LAI-2000 (61 pts * 3 Repeat)
Maximum	1.68	3.52	3.36	1.56	3.85	3.3
Minimum	1.37	2.9	3.19	1.05	2.87	3.18
Mean	1.533	3.186	3.275	1.282	3.248	3.243
SD	0.12	0.23	0.12	0.2	0.39	0.06
System bias (ε) *	–	*1.653*	*1.724*	=	*1.966*	*1.962*

* The LAI were measured at 5 points, in four directions, and repeated two to three times for every plot. The system bias (ε) was calculated by (LAI-2000 LAI_e- DHP LAI_{DHP}).

According to Table A2, the system bias was set to 1.83 for the DHP method. The correction parameters required to convert LAI_e to LAI_t were set as follows: the needle-to-shoot area ratio (γ_e) was set to 1.1 according to the results of the destructive sampling conducted in August 2015. The clumping index Ω was produced by the TRAC instrument and set to 0.8. The value of the woody-to-total area ratio (α) for *Cunninghamia lanceolata* was derived from the destructive samples used to calculate biomass and was set to 0.2. An illustration of the data processing workflow may be useful for understanding how we unified the LAI field data measured by different instruments, as shown in Figure A5.
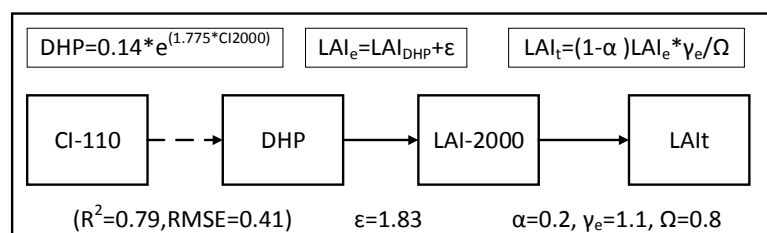
Figure A5. Flowchart of LAI field data processing procedures. Before January 2007, monthly LAI was measured using a CI-110 instrument, and a DHP instrument was used afterwards.

References

1. Waring, R.H.; Schlesinger, W.H. *Forest Ecosystems: Concepts and Management*; Academic Press: Orlando, FL, USA, 1985; p. 75.
2. Dixon, R.K.; Brown, S.; Houghton, R.E.A.; Solomon, A.; Trexler, M.; Wisniewski, J. Carbon pools and flux of global forest ecosystems. *Science (Washington)* **1994**, *263*, 185–189. [CrossRef] [PubMed]
3. Schimel, D.; Stephens, B.B.; Fisher, J.B. Effect of increasing CO_2 on the terrestrial carbon cycle. *Proc. Natl. Acad. Sci. USA* **2015**, *112*, 436–441. [CrossRef] [PubMed]
4. Pan, Y.; Birdsey, R.A.; Fang, J.; Houghton, R.; Kauppi, P.E.; Kurz, W.A.; Phillips, O.L.; Shvidenko, A.; Lewis, S.L.; Canadell, J.G. A large and persistent carbon sink in the world's forests. *Science* **2014**, *333*, 988–993. [CrossRef] [PubMed]
5. Reich, P.B. Biogeochemistry: Taking stock of forest carbon. *Nat. Clim. Chang.* **2016**, *1*, 346–347. [CrossRef]
6. Guyot, G.; Guyon, D.; Riom, J. Factors affecting the spectral response of forest canopies: A review. *Geocarto Int.* **1989**, *4*, 3–18. [CrossRef]
7. Vermote, E.F.; Tanré, D.; Deuze, J.L.; Herman, M.; Morcette, J.-J. Second simulation of the satellite signal in the solar spectrum, 6s: An overview. *IEEE Trans. Geosci. Remote Sens.* **1997**, *35*, 675–686. [CrossRef]
8. Samanta, A.; Ganguly, S.; Vermote, E.; Nemani, R.R.; Myneni, R.B. Why is remote sensing of Amazon forest greenness so challenging? *Earth Interact.* **2012**, *16*, 1–14. [CrossRef]
9. Xiao, X.; Braswell, B.; Zhang, Q.; Boles, S.; Frolking, S.; Moore, B. Sensitivity of vegetation indices to atmospheric aerosols: Continental-scale observations in northern asia. *Remote Sens. Environ.* **2003**, *84*, 385–392. [CrossRef]

10. Galvão, L.S.; dos Santos, J.R.; Roberts, D.A.; Breunig, F.M.; Toomey, M.; de Moura, Y.M. On intra-annual evi variability in the dry season of tropical forest: A case study with MODIS and hyperspectral data. *Remote Sens. Environ.* **2011**, *115*, 2350–2359. [CrossRef]

11. Maeda, E.E.; Heiskanen, J.; Aragão, L.E.; Rinne, J. Can MODIS evi monitor ecosystem productivity in the Amazon rainforest? *Geophys. Res. Lett.* **2014**, *41*, 7176–7183. [CrossRef]

12. Maeda, E.E.; Galvão, L.S. Sun-sensor geometry effects on vegetation index anomalies in the Amazon rainforest. *GISci. Remote Sens.* **2015**, *52*, 332–343. [CrossRef]

13. Bi, J.; Knyazikhin, Y.; Choi, S.; Park, T.; Barichivich, J.; Ciais, P.; Fu, R.; Ganguly, S.; Hall, F.; Hilker, T. Sunlight mediated seasonality in canopy structure and photosynthetic activity of Amazonian rainforests. *Environ. Res. Lett.* **2015**, *10*, 064014. [CrossRef]

14. Moura, Y.M.; Galvão, L.S.; dos Santos, J.R.; Roberts, D.A.; Breunig, F.M. Use of MISR/Terra data to study intra- and inter-annual EVI variations in the dry season of tropical forest. *Remote Sens. Environ.* **2012**, *127*, 260–270. [CrossRef]

15. Lyapustin, A.I.; Wang, Y.; Laszlo, I.; Hilker, T.; Hall, F.G.; Sellers, P.J.; Tucker, C.J.; Korkin, S.V. Multi-angle implementation of atmospheric correction for MODIS (MAIAC): 3. Atmospheric correction. *Remote Sens. Environ.* **2012**, *127*, 385–393. [CrossRef]

16. Jones, M.O.; Kimball, J.S.; Nemani, R.R. Asynchronous Amazon forest canopy phenology indicates adaptation to both water and light availability. *Environ. Res. Lett.* **2014**, *9*, 124021. [CrossRef]

17. Goward, S.N.; Huemmrich, K.F. Vegetation canopy par absorptance and the normalized difference vegetation index: An assessment using the sail model. *Remote Sens. Environ.* **1992**, *39*, 119–140. [CrossRef]

18. Ollinger, S.V. Sources of variability in canopy reflectance and the convergent properties of plants. *New Phytol.* **2011**, *189*, 375–394. [CrossRef] [PubMed]

19. Asner, G.P. Biophysical and biochemical sources of variability in canopy reflectance. *Remote Sens. Environ.* **1998**, *64*, 234–253. [CrossRef]

20. Jacquemoud, S.; Verhoef, W.; Baret, F.; Bacour, C.; Zarco-Tejada, P.J.; Asner, G.P.; François, C.; Ustin, S.L. Prospect+ sail models: A review of use for vegetation characterization. *Remote Sens. Environ.* **2009**, *113*, S56–S66. [CrossRef]

21. Eriksson, H.M.; Eklundh, L.; Kuusk, A.; Nilson, T. Impact of understory vegetation on forest canopy reflectance and remotely sensed lai estimates. *Remote Sens. Environ.* **2006**, *103*, 408–418. [CrossRef]

22. Jordan, C.F. Derivation of leaf-area index from quality of light on the forest floor. *Ecology* **1969**, *50*, 663–666. [CrossRef]

23. Samanta, A.; Knyazikhin, Y.; Xu, L.; Dickinson, R.E.; Fu, R.; Costa, M.H.; Saatchi, S.S.; Nemani, R.R.; Myneni, R.B. Seasonal changes in leaf area of Amazon forests from leaf flushing and abscission. *J. Geophys. Res. Biogeosci.* **2012**, *117*. [CrossRef]

24. Asner, G.P.; Alencar, A. Drought impacts on the Amazon forest: The remote sensing perspective. *New Phytol.* **2010**, *187*, 569–578. [CrossRef] [PubMed]

25. Monteith, J.L.; Ross, J. *The Radiation Regime and Architecture of Plant Stands*; Springer: Dordrecht, The Netherlands, 1981; p. 344.

26. Asner, G.P.; Wessman, C.A.; Schimel, D.S.; Archer, S. Variability in leaf and litter optical properties: Implications for BRDF model inversions using AVHRR, MODIS, and MISR. *Remote Sens. Environ.* **1998**, *63*, 243–257. [CrossRef]

27. Doughty, C.E.; Goulden, M.L. Seasonal patterns of tropical forest leaf area index and CO_2 exchange. *J. Geophys. Res. Biogeosci.* **2008**, *113*. [CrossRef]

28. Wu, J.; Albert, L.P.; Lopes, A.P.; Restrepo-Coupe, N.; Hayek, M.; Wiedemann, K.T.; Guan, K.; Stark, S.C.; Christoffersen, B.; Prohaska, N. Leaf development and demography explain photosynthetic seasonality in Amazon evergreen forests. *Science* **2016**, *351*, 972–976. [CrossRef] [PubMed]

29. Horler, D.; Ahern, F. Forestry information content of thematic mapper data. *Int. J. Remote Sens.* **1986**, *7*, 405–428. [CrossRef]

30. Cohen, W.B.; Spies, T.A.; Fiorella, M. Estimating the age and structure of forests in a multi-ownership landscape of western Oregon, USA. *Int. J. Remote Sens.* **1995**, *16*, 721–746. [CrossRef]

31. Jakubauskas, M.E. Thematic Mapper characterization of lodgepole pine seral stages in Yellowstone National Park, USA. *Remote Sens. Environ.* **1996**, *56*, 118–132. [CrossRef]

32. Song, C.; Schroeder, T.A.; Cohen, W.B. Predicting temperate conifer forest successional stage distributions with multitemporal landsat thematic mapper imagery. *Remote Sens. Environ.* **2007**, *106*, 228–237. [CrossRef]

33. Nilson, T.; Peterson, U. Age dependence of forest reflectance: Analysis of main driving factors. *Remote Sens. Environ.* **1994**, *48*, 319–331. [CrossRef]

34. Eckenwalder, J.E. *Conifers of the World: The Complete Reference*; Timber Press: Portland, OR, USA, 2009.

35. Chen, J.; Black, T.; Adams, R. Evaluation of hemispherical photography for determining plant area index and geometry of a forest stand. *Agric. For. Meteorol.* **1991**, *56*, 129–143. [CrossRef]

36. Wagner, S. Calibration of grey values of hemispherical photographs for image analysis. *Agric. For. Meteorol.* **1998**, *90*, 103–117. [CrossRef]

37. Englund, S.R.; O'brien, J.J.; Clark, D.B. Evaluation of digital and film hemispherical photography and spherical densiometry for measuring forest light environments. *Can. J. For. Res.* **2000**, *30*, 1999–2005. [CrossRef]

38. Song, G.-Z.M.; Doley, D.; Yates, D.; Chao, K.-J.; Hsieh, C.-F. Improving accuracy of canopy hemispherical photography by a constant threshold value derived from an unobscured overcast sky. *Can. J. For. Res.* **2013**, *44*, 17–27. [CrossRef]

39. Liu, Z.; Jin, G.; Chen, J.M.; Qi, Y. Evaluating optical measurements of leaf area index against litter collection in a mixed broadleaved-Korean pine forest in China. *Trees* **2015**, *29*, 59–73. [CrossRef]

40. Tarantola, S.; Becker, W. Simlab software for uncertainty and sensitivity analysis. In *Handbook of Uncertainty Quantification*; Ghanem, R., Higdon, D., Owhadi, H., Eds.; Springer: Cham, Switzerland, 2016; pp. 1–21.

41. Li, X.; Strahler, A.H.; Woodcock, C.E. Hybrid geometric optical-radiative transfer approach for modeling albedo and directional reflectance of discontinuous canopies. *IEEE Trans. Geosci. Remote Sens.* **1995**, *33*, 466–480.

42. Ni, W.; Li, X.; Woodcock, C.E.; Caetano, M.R.; Strahler, A.H. An analytical hybrid gort model for bidirectional reflectance over discontinuous plant canopies. *IEEE Trans. Geosci. Remote Sens.* **1999**, *37*, 987–999.

43. Li, X.; Strahler, A.H. Geometric-optical modeling of a conifer forest canopy. *IEEE Trans. Geosci. Remote Sens.* **1985**, *23*, 705–721. [CrossRef]

44. Li, X.; Strahler, A.H. Geometric-optical bidirectional reflectance modeling of a conifer forest canopy. *IEEE Trans. Geosci. Remote Sens.* **1986**, *24*, 906–919. [CrossRef]

45. Li, X.; Strahler, A.H. Geometric-optical bidirectional reflectance modeling of the discrete crown vegetation canopy: Effect of crown shape and mutual shadowing. *IEEE Trans. Geosci. Remote Sens.* **1992**, *30*, 276–292. [CrossRef]

46. Serra, J. The boolean model and random sets. *Comput. Graph. Image Process.* **1980**, *12*, 99–126. [CrossRef]

47. Li, X.; Strahler, A.H. Modeling the gap probability of a discontinuous vegetation canopy. *IEEE Trans. Geosci. Remote Sens.* **1988**, *26*, 161–170. [CrossRef]

48. Ni, W.; Li, X.; Woodcock, C.E.; Roujean, J.-L.; Davis, R.E. Transmission of solar radiation in boreal conifer forests: Measurements and models. *J. Geophys. Res. All Ser.* **1997**, *103*, 29555–29566. [CrossRef]

49. Song, C.; Woodcock, C.E.; Li, X. The spectral/temporal manifestation of forest succession in optical imagery: The potential of multitemporal imagery. *Remote Sens. Environ.* **2002**, *82*, 285–302. [CrossRef]

50. Zhongkun, X.U.; Qingqian, X.U.; Rong, J. The characters of leaf area and net photosynthesis efficiency of needle at different parts and in different leaf age of *Cunninghamia lanceolata*. *Hunan For. Sci. Technol.* **2008**, *41*, 1–4.

51. Saltelli, A.; Bolado, R. An alternative way to compute fourier amplitude sensitivity test (FAST). *Comput. Stat. Data Anal.* **1998**, *26*, 445–460. [CrossRef]

52. Shi, H.; Xiao, Z.; Liang, S.; Zhang, X. Consistent estimation of multiple parameters from MODIS top of atmosphere reflectance data using a coupled soil-canopy-atmosphere radiative transfer model. *Remote Sens. Environ.* **2016**, *184*, 40–57. [CrossRef]

53. Saltelli, A.; Annoni, P.; Azzini, I.; Campolongo, F.; Ratto, M.; Tarantola, S. Variance based sensitivity analysis of model output. Design and estimator for the total sensitivity index. *Comput. Phys. Commun.* **2010**, *181*, 259–270. [CrossRef]

54. Saltelli, A.; Tarantola, S.; Chan, K.P.-S. A quantitative model-independent method for global sensitivity analysis of model output. *Technometrics* **1999**, *41*, 39–56. [CrossRef]

55. Saltelli, A.; Tarantola, S.; Campolongo, F.; Ratto, M. Sensitivity analysis in practice. *J. Am. Stat. Assoc.* **2004**, *101*, 398–399.

56. Li, X.; Gao, F.; Wang, J.; Zhu, Q. Uncertainty and sensitivity matrix of parameters in inversion of physical BRDF model. *J. Remote Sens.* **1997**, *1*, 161–172.

57. Tarantola, A. *Inverse Problem Theory and Methods for Model Parameter Estimation*; Society for Industrial and Applied Mathematics (SIAM): Philadelphia, PA, USA, 2005.

58. Nocedal, J.; Wright, S.J. *Sequential Quadratic Programming*; Springer: New York, NY, USA, 2006.

59. Lin, Z.F.; Ehleringer, J. Changes in spectral properties of leaves as related to chlorophyll content and age of papaya. *Photosynthetica* **1982**, *16*, 520–525.

60. Roberts, D.A.; Nelson, B.W.; Adams, J.B.; Palmer, F. Spectral changes with leaf aging in Amazon caatinga. *Trees* **1998**, *12*, 315–325. [CrossRef]

61. Rock, B.N.; Williams, D.L.; Moss, D.M.; Lauten, G.N.; Kim, M. High-spectral resolution field and laboratory optical reflectance measurements of red spruce and eastern hemlock needles and branches. *Remote Sens. Environ.* **1994**, *47*, 176–189. [CrossRef]

62. Gausman, H.W.; Allen, W.A.; Cardenas, R.; Richardson, A.J. Reflectance discrimination of cotton and corn at four growth stages. *Agron. J.* **1973**, *65*, 194–198. [CrossRef]

63. Chavanabryant, C.; Malhi, Y.; Wu, J.; Asner, G.P.; Anastasiou, A.; Enquist, B.J.; Cosio Caravasi, E.G.; Doughty, C.E.; Saleska, S.R.; Martin, R.E. Leaf aging of Amazonian canopy trees as revealed by spectral and physiochemical measurements. *New Phytol.* **2017**, *214*, 1049–1063. [CrossRef] [PubMed]

64. Samanta, A.; Ganguly, S.; Myneni, R.B. MODIS enhanced vegetation index data do not show greening of Amazon forests during the 2005 drought. *New Phytol.* **2011**, *189*, 11–15. [CrossRef] [PubMed]

65. Samanta, A.; Costa, M.H.; Nunes, E.L.; Vieira, S.A.; Xu, L.; Myneni, R.B. Comment on drought-induced reduction in global terrestrial net primary production from 2000 through 2009. *Science* **2011**, *333*, 1093. [CrossRef] [PubMed]

66. Xu, L.; Samanta, A.; Costa, M.H.; Ganguly, S.; Nemani, R.R.; Myneni, R.B. Widespread decline in greenness of Amazonian vegetation due to the 2010 drought. *Geophys. Res. Lett.* **2011**, *38*, 490–500. [CrossRef]

67. Toomey, M.; Roberts, D.; Nelson, B. The influence of epiphylls on remote sensing of humid forests. *Remote Sens. Environ.* **2009**, *113*, 1787–1798. [CrossRef]

68. Xiaoquan, Z.; Deying, X. Seasonal changes and daily courses of photosynthetic characteristics of 18-year-old chinese fir shoots in relation to shoot ages and positions within tree crown. *Sci. Silvae Sin.* **2000**, *36*, 19–26.

69. Wu, J.; Serbin, S.P.; Xu, X.; Albert, L.P.; Chen, M.; Meng, R.; Saleska, S.R.; Rogers, A. The phenology of leaf quality and its within-canopy variation are essential for accurate modeling of photosynthesis in tropical evergreen forests. *Glob. Chang. Biol.* **2017**, *23*, 4814–4827. [CrossRef] [PubMed]

70. Frazer, G.W.; Fournier, R.A.; Trofymow, J.A.; Hall, R.J. A comparison of digital and film fisheye photography for analysis of forest canopy structure and gap light transmission. *Agric. For. Meteorol.* **2001**, *109*, 249–263. [CrossRef]

71. Zhang, Y.; Chen, J.M.; Miller, J.R. Determining digital hemispherical photograph exposure for leaf area index estimation. *Agric. For. Meteorol.* **2005**, *133*, 166–181. [CrossRef]